Impact of different event reconstruction methods on diffractive physics studied at the Electron-Ion Collider

A Thesis

submitted to
Indian Institute of Science Education and Research Pune
in partial fulfillment of the requirements for the
BS-MS Dual Degree Programme

by

Athira K V

Indian Institute of Science Education and Research Pune
Dr. Homi Bhabha Road,
Pashan, Pune 411008, INDIA.

May, 2020

Supervisor: Dr. Abhay Deshpande

Certificate

This is to certify that this dissertation entitled *Impact of different event reconstruction methods on diffractive physics studied at the Electron-Ion Collider* towards the partial fulfilment of the BS-MS dual degree programme at the Indian Institute of Science Education and Research, Pune represents study/work carried out by Athira K V at Stony Brook University under the supervision of Dr. Abhay Deshpande, Professor, Stony Brook University, during the academic year 2019-2020.

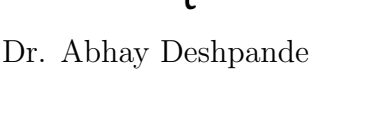

Dr. Abhay Deshpande

Athira K V

Committee:

Dr. Abhay Deshpande

Dr. Tobias Toll

Dr. Sourabh Dube

This thesis is dedicated to my mother, Chandrika.

Declaration

I hereby declare that the matter embodied in the report entitled *Impact of different event reconstruction methods on diffractive physics studied at the Electron-Ion Collider*, is the result of the work carried out by me at Stony Brook University under the supervision of Dr. Abhay Deshpande and the same has not been submitted elsewhere for any other degree.

Dr. Abhay Deshpande

Athira K V

Acknowledgments

I would like to express my sincere gratitude to Professor Abhay Deshpande for providing me a great opportunity to work on an exciting project for the upcoming Electron-Ion Collider(EIC). It was his enthusiastic encouragement and useful critiques that kept me motivated to work hard. I am also grateful to Dr. Barak Schmookler for his extremely valuable inputs and helpful discussions, which helped the project to progress. I would like to extend my deepest gratitude to Dr. Tobias Toll for his careful and skilled guidance and support during the initial few months of my work and stay at IIT Delhi.

I would like to thank Prof. Bhas Bapat, Prof. Seema Sharma, Prof. Sourabh Dube, and the whole of the IISER EHEP group for providing useful suggestions and constant guidance for the past three years. I would like to convey my special thanks to Prof. Christine Aidala of the University of Michigan for introducing to me the science of the novel machine for understanding QCD.

I am indebted to the Centre for Frontiers in Nuclear Science (CFNS) at Stony Brook University, and Kishore Vaigyanik Prolsahan Yojana (KVPY) for providing me financial support throughout the duration of the project. I would like to recognize the invaluable assistance that the HEP group at IIT Delhi and CFNS at SBU have provided me for the successful completion of my project. I am incredibly grateful to Dr. Roli Esha at SBU for being there for me as a friend, mentor, and motivator. Thanks to my mom, dad, and sisters for their relentless support and encouragement. Last but not least, thanks to all my friends whom I could always count on.

Abstract

Diffractive Deep Inelastic Scattering – defined by a colorless exchange between the target nucleus and the incoming electron – is sensitive to the geometric structure of hadrons, and hence can be used as a probe for exploring the mystery of confinement and saturation. Experimentally, this process manifests itself by a rapidity gap in the detector between the outgoing nucleus/remnants and the diffractively produced system. The thesis mainly discusses three complementary event kinematic reconstruction methods for exclusive diffractive events: the Scattered Electron method, the Jacquet Blondel method, and the Double Angle method; and we will assess their impact on the physics studied in different kinematic regimes. The simulation studies are performed using an e-A event generator made exclusively for diffractive events – Sartre. The output of the Sartre generator is passed to both a fast simulation package (eic-smear) as well as a full Geant4 EIC detector simulation to perform the kinematics reconstruction studies. In addition, for diffractive vector meson production, there is a known dependence of the angular distribution of the vector meson decay products on the polarization of the virtual photon. The method by which this effect is incorporated into the Sartre event generator is also described.

Contents

List of Figures

List of Tables

Chapter 1

Introduction

The twentieth century has been a fascinating era for physics. With Max Planck's theory of quantum physics [1] which aided in the formulation of quantum mechanics, and Einstein's theory of relativity [2], various research areas in theoretical and experimental physics flourished. A remarkable incident in experimental physics that led to the birth of particle physics as we know it today is the Rutherford's alpha scattering experiment [3]. Several theories were later put forward, anticipating the structure of the atom. We have come a long way from the plum pudding model to the Standard Model of particle physics (Figure 1.1)

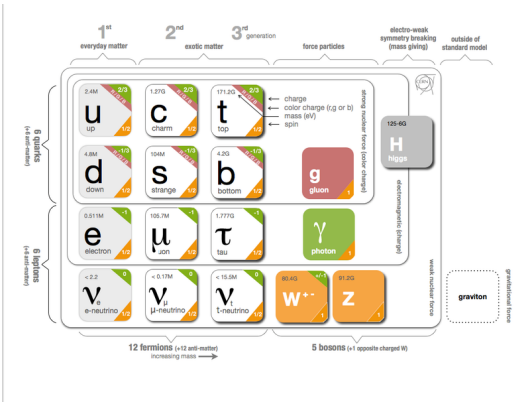

Figure 1.1: Standard Model

The discovery of neutron in nuclear fission [4] gave rise to the idea of protons and neutrons being the constituents of a nucleus and held together by the strongest force in nature, the nuclear force.

With advancements in technology, several high energy collider experiments were conducted, which prompted the understanding that proton is an extended object, unlike electron, which we know even today as a point particle. Nuclear physics is concerned with the study of the atomic nuclei, nucleons (protons and neutrons) within, and interactions that account for almost all of the mass of the visible universe. Further experiments in the field of nuclear physics led to the discovery of quarks and gluons, which the nucleons are composed of [5]. A theory was formulated to explain the phenomena of strong interaction where the quarks and gluons are bound together by strong nuclear force - the theory of quantum chromodynamics (QCD) [9][8]. One of the most compelling goals of nuclear physics is to understand the interactions which hold the constituents, and the emergence of the nucleons and nuclei from the properties and dynamics of the constituent quark and gluons[12].

Unlike in quantum electrodynamics where the force carrying photons are electrically neutral, QCD attributes "color charge" to gluons. Hence, gluons can interact with one another, unlike photons, and this gives rise to a significant fraction of the nucleon mass and a regime of matter where gluons dominate, which is yet to be explored. In colliders such as HERA at DESY, RHIC at BNL and LHC at CERN nucleons and/or nuclei collide at near the speed of light. A new experimental facility proposed at BNL , the Electron-Ion Collider (EIC) will manifest a wide variety of unanswered questions in this regime [10].

In an EIC, the structure of hadrons is probed by the process of Deep Inelastic Scattering (DIS) [6]. DIS is a process by which the participating nucleon/nucleus is scanned by leptons such as electron, muon, or neutrino. At higher energies of e-A collisions, the process helps in probing regions of higher gluon density. However, in order to prevent the uncontrollable growth in the strength of the strong nucleon-nucleon interaction, this gluon density has to be saturated at some point. With EIC, we propose to explore this less-unexplored state of matter facilitated by heavy nuclei collisions that would amplify the gluon density being probed. In the 2007 Nuclear Physics Long Range Plan [11], the EIC was delegated as "embodying the vision for reaching the next QCD frontier". The following are the pressing questions which we expect to answer in detail once EIC comes in to play.

- How are the position and spins of sea quarks and gluons, inside a nuclei, distributed in space and momentum?
- When/How/Where does the gluon saturation set in?
- How are the distributions of quarks and gluons, and their interaction affected by the

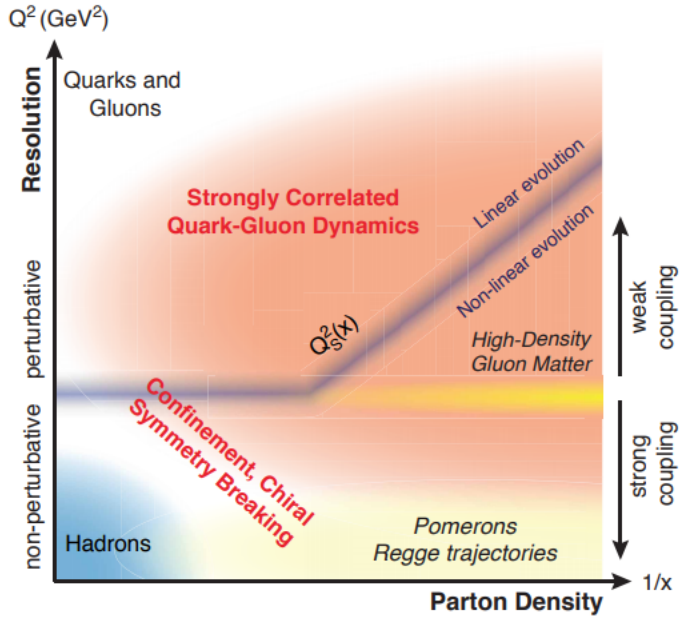

Figure 1.2: Different physics regimes under the study of EIC [10]

nuclear environment?

We argue [10] that EIC is the ultimate machine to answer these due to the accessibility to the kinematic regimes of interest, use of polarized electron and nucleon beams, heavy nuclei collisions at high luminosity, which no other existing collider offers. Various physics studies that can be done at different physics regimes with the EIC facility has been summarized in the figure (Figure 1.2).

1.1 Diffractive Physics at EIC

The HERA e + p collider showed a surprising 15 percent of the total DIS cross-section[10] contributed by the so called diffractive events. The diffractive events are the only known class of events which give a revelation about the gluon spatial distribution inside nuclei. Diffractive Deep Inelastic Scattering (DDIS) is defined by a colorless exchange between the target nucleus and the incoming electron. Experimentally, such a scattering manifests itself as a rapidity gap in the detector between the outgoing nucleus/remnants and the diffractively produced system. These events are sensitive to the geometric structure of hadrons,

and hence can be used as probes for exploring the mystery of confinement and saturation. Deep Inelastic Scattering can be inclusive (only the leptonic final state is detected), semi-inclusive (a portion of the hadronic final state detected in coincidence with the scattered lepton) and exclusive (all the final state particles are detected). My thesis work focuses on the three complementary event kinematic reconstruction methods- Scattered electron Method, Jacquet Blondel Method and the Double angle Method, and their impact on the physics studied at different kinematic regimes, focusing on exclusive diffractive events.

Diffractive events can be coherent(the nucleus stays intact) and incoherent (the nucleus excites and breaks up). In diffractive vector meson production, e + A $\rightarrow$ e' + A' + V, where V = J/ψ , ρ , ϕ or γ , the momentum transfer t at the hadronic vertex can be measured even in the case of e A collisions when the four-momentum of the outgoing nucleus is difficult to access. Also, these processes are experimentally unclouded as there is only one new final state particle, the vector meson (VM).

Sartre is an event generator for exclusive diffractive vector meson production [20]. Using Sartre, coherent diffractive events of J/ψ VM production were generated and kinematic reconstruction done using the three different methods. As it turns out that the scattered electron method provides a greater concurrence as compared to other methods, we have looked at the specific case where J/ψ decays to e^+ e^- pair and if the primary electron can be well distinguished from this decay product. Initially working at the generator level, moving to detector smearing through a package called *eic-smear* [13] and further trying to develop a more realistic picture using full GEANT4 detector simulations for the kinematic reconstruction studies for exclusive diffractive events have been described in the thesis. Analysis and interpretations on how the reconstruction methods affect different x-Q^2 regimes have been explained. Furthermore, what detector designs and locations would be helpful in pursuing the targeted physics at EIC have also been investigated.

Chapter 2

Deep Inelastic Scattering

It was in the year 1969 when electrons accelerated to about 7 GeV scattered off the hydrogen [7], we saw the first Deep Inelastic Scattering (DIS) experiment. The term "deep" indicates that the energies were so high that the participating proton structure could be probed to a resolution of a fraction of the radius of a proton. "Inelastic" is conveying how the proton breaks up, after the collision, into fragments producing plenty of new particles. Thus we realize DIS (where you scatter leptons off hadrons) is the most powerful and cleanest process to study the structure of hadrons. In this chapter, the different kinematic variables of a DIS process are discussed. Also, various methods used to reconstruct these event kinematic variables have been explained in detail. We will also see a specific case of DIS called diffractive deep inelastic scattering (DDIS), and how relevant that is in the current research.
As shown in Figure 2.1, deep inelastic scattering is mediated by the exchange of a virtual

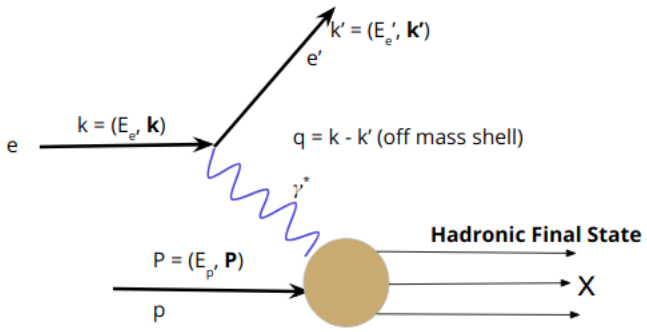

Figure 2.1: Deep Inelastic Scattering

photon (in general, the mediators of DIS are electro-weak gauge bosons). The higher the energy of the virtual photon, the higher the resolution with which we can probe the nucleus/proton. Based on the measured final states in a DIS process, it can be classified as inclusive, semi-inclusive, or exclusive. Refer to the following table for details.

Table 2.1: Characteristic measurements at EIC [15]

Measurement	Beam	Measured Final State
Inclusive DIS	e+p	scattered e^-
Semi-Inclusive DIS	e+p	scattered e^- identified hadron
DVCS	e+p	scattered e^- photon scattered p
DVMP with J/Ψ	e+p	scattered e^- e^- + e^+ from J/Ψ decay scattered p
Diffraction	e+A	scattered e^- rapidity gap n from nuclear dissociation

2.1 DIS Kinematics

Let us consider an inclusive DIS process (See Figure 2.1) where we perform a sum over all the hadronic final states X.

$$e^-(k) + p(P) \rightarrow e^-(k') + X \tag{2.1}$$

The square of momentum transfer at the lepton vertex is the mass of virtual photon.

$$q^2 = (k - k')^2 = -Q^2 \tag{2.2}$$

Therefore, Q^2 can be written in terms of the four momenta of the participating electron as,

$$Q^2 = -(k - k')^2 = -2m_e^2 + 2EE' - 2kk'cos\theta \tag{2.3}$$

where θ is the scattering angle of the electron. In DIS, the mass of the electron can be neglected and the equation for Q^2 reduces to,

$$Q^2 \simeq 2EE'(1 - cos\theta) = 4EE'sin^2\frac{\theta}{2} \tag{2.4}$$

Hence, Q^2 is always positive and can be considered as a measure of the virtuality of the photon.
Another important Lorentz-invariant quantity is the Bjorken x.

$$x = \frac{Q^2}{2P.\ q} \tag{2.5}$$

Bjorken x is the fraction of the proton's total momentum as carried by the parton. Therefore,

$$0 \leq x \leq 1 \tag{2.6}$$

and $x = 1$ corresponds to the elastic limit.
Since x is a measure of the momentum fraction, a wide range of x is essential to cover the regimes dominated by valence quarks to sea-quarks and gluons. As Q^2 is considered as a scale at which the partons can be resolved, a large lever arm in Q^2 is required to investigate the scale violation in parton distribution.
Now we define the inelasticity, y, as

$$y = \frac{P.\ q}{P.\ k} \tag{2.7}$$

In a frame where the proton is at rest, the four momenta of incoming electron, the target proton and the momenta transferred to the photon can be written as, $k = (E, 0, 0, E)$, $P = (m_p, 0, 0, 0)$, and $q = (E - E', \mathbf{k} - \mathbf{k'})$ respectively. In this case, y takes the form,

$$y = 1 - \frac{E'}{E} \tag{2.8}$$

and, is defined as the fractional energy loss of the incoming electron as measured in the frame where proton is initially at rest. Since we have the total energy of the hadronic system to be greater than the energy of the initial proton, the electron must lose energy in the scattering process, hence constraining the value of y.

$$0 \leq y \leq 1 \tag{2.9}$$

Another related quantity ν can be defined as,

$$\nu = \frac{P.\ q}{m_p} \tag{2.10}$$

where m_p is the mass of the proton. In the frame where we have target proton at rest, ν is just the difference in the energies of the incoming electron and scattered electron.

$$\nu = E - E' \tag{2.11}$$

We have defined four different Lorentz-invariant kinematic variables. However, it can be shown that at fixed centre-of-mass energy, these variables are not all independent. For example, the scaling variables x and y can be expressed as,

$$x = \frac{Q^2}{2m_p\nu} \tag{2.12}$$

$$y = \frac{2m_p}{s - m_p^2}\nu \tag{2.13}$$

where s is the centre-of-mass energy expressed using the four momenta as,

$$s = (k + P)^2 = k^2 + P^2 + 2k.P \simeq m_p^2 + 2k.P \tag{2.14}$$

Finally, from equations (2.12) and (2.13), Q^2 can be written as,

$$Q^2 = (s - m_p^2)xy \tag{2.15}$$

Hence, for a fixed centre-of-mass energy, the interaction kinematics can be completely defined by any two of the four Lorentz-invariant kinematic variables x, Q^2, y and ν (except y and ν as they are not independent), for instance, (E', θ), (x, y), or (x, Q^2).
Another important quantity to be defined is the invariant mass of the hadronic final state, W. As only the outgoing electron is measured in case of inclusive DIS, W is also called the missing mass.

$$W^2 = m_X^2 = (P + q)^2 \tag{2.16}$$

The following picture (Figure 2.2) from Quarks and leptons, Halzen and Martin [8] shows the $ep \to eX$ cross-section as a function of W. In the case of elastic scattering, proton stays intact ($ep \to ep$) and $W = m_p$ as shown by the leftmost peak in the picture. At slightly

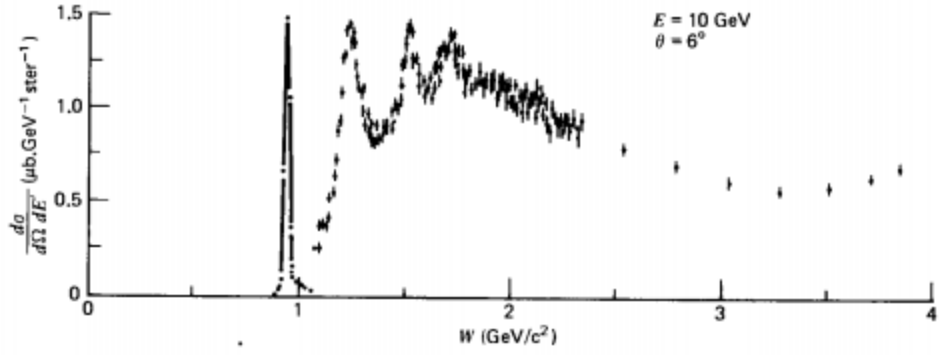

Figure 2.2: ep→ eX cross-section as a function of W

higher W (elastic region), there are excited states and the discrete peaks correspond to resonances. When we move to the deep inelastic region, we reach a continuum corresponding to complicated multi-particle final states and thus the distribution in W is smooth.

2.2 Diffractive Deep Inelastic Scattering (DDIS)

We are familiar with the phenomenon of diffraction arising due to the constructive and destructive interference of waves in optics. When a plane monochromatic wave passes a circular obstacle, the following diffraction pattern is seen (image on the left)(See Figure 2.3). The minima and maxima give information about the size of the obstacle in case of small angle diffraction. The same analogy can be traced to QCD as well. Interestingly, in an elastic scattering process where the target proton/nucleus stays intact after scattering by a lepton or hadron (projectile), the differential cross-section as a function of the mandelstam t, which is the square of the momentum transfer between the target and the projectile, yields a similar distribution. (See the image on the right in Figure 2.3).

Hence, the information derived from the maxima and minima in the distribution pattern can be used to study the structure of the target, thereby helping in the spatial imaging of the nucleons.
A diffractive process in QCD is defined

- experimentally by the presence of a rapidity gap in the detector, and

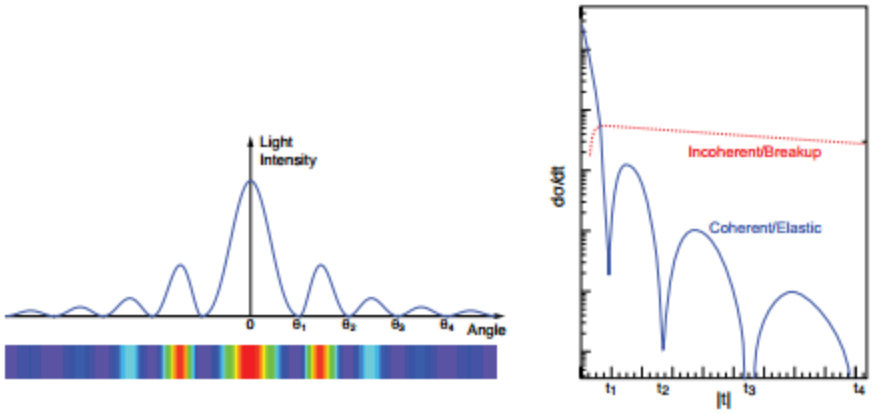

Figure 2.3: The picture on the left shows the diffraction pattern produced by a spherical aperture. On the right is the cross-section of the diffractive processes as a function of the mandelstam t [10]

- theoretically by the colorless exchange of gluons between the projectile and the target proton/nucleus.

Therefore, even if the target breaks up, we still get a diffractive process as long as there is a rapidity gap in the detector. In a coherent diffractive process, the target stays intact after the scattering, and in an incoherent diffractive event, the target breaks up into fragments forming a multi-particle final state.
In diffractive deep inelastic scattering (DDIS), the projectile electron scatters off the proton/nucleus without net color exchange. Had it been a color exchange, according to the

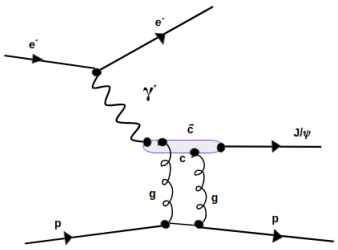

Figure 2.4: Diffractive Vector Meson Production with the gluon exchange

color confinement in QCD, this exchange would have to fragment into a shower of hadrons so as to fill up the rapidity gap. Hence, these processes are a powerful indication of color confinement. At the leading order in perturbative QCD, it is this color singlet exchange of two gluons implying that these processes relate to the square of the distribution function of

target gluons, aiding in unraveling the mystery of gluon saturation, as shown in Figure 2.4.

Also, referring to the Fig. 2.3, the Fourier transform of the t distribution would give the gluon spatial distribution inside the nucleus, hinting to the geometric structure of hadrons [17][20]. Therefore, diffractive events are outstanding probes to investigate the physics mentioned above, at EIC.

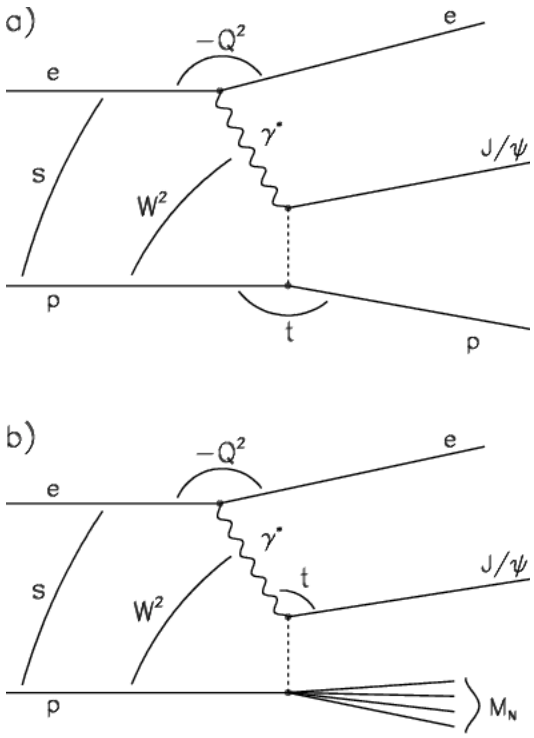

Figure 2.5: a)Coherent diffractive vector meson production, b) incoherent diffractive vector meson production

2.2.1 Deeply Virtual Meson Produciton (DVMP)

In exclusive diffraction, an additional striking advantage comes through the process of exclusive vector meson production. These processes provide a handle to study small x gluon distributions, and as they are experimentally unclouded (as there are a few final state particles in which the vector meson being the only new one), reconstruction of the mandelstam t becomes less tedious. Also, based on recent phenomenological studies, exclusive J/ψ production is a relevant tool for understanding the event fluctuations and average density profiles

for both protons and nuclei. My thesis work mainly focuses on the exclusive diffractive production of J/ψ and its subsequent decay to e^+ and e^-, as shown in Figure 2.5 a).

Chapter 3

Detector Concepts and Simulations

The upcoming Electron-Ion Collider (EIC) is a machine that would unveil the mystery of strong force in nature. EIC is going to be the first-ever collider to have polarized lepton and hadron beams. It is a next-generation facility to conduct outstanding studies on quantum chromodynamics and is considered as top priority nuclear physics facility. The two possible realizations for EIC were JLEIC at the Thomas Jefferson Accelerator Laboratory (JLab), Virginia, USA and, eRHIC at the Brookhaven National Laboratory (BNL), New York, USA. On the 9th of January 2020, the U.S Department of Energy selected BNL as the site for the EIC [16], where the proposed design is to upgrade the existing Relativistic Heavy Ion Collider (RHIC), and collide light to heavy nuclei and polarized protons with spin-polarized electrons. As far as the detector is concerned, there are currently four proposals for the central detector, as shown in Figure 3.1.

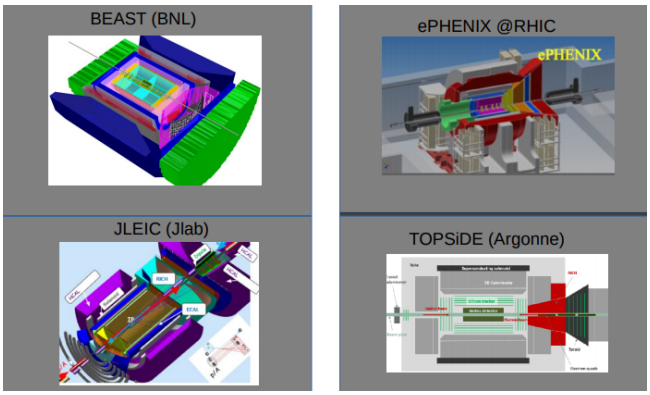

Figure 3.1: Four proposed central detectors for EIC

There have been recent studies on reusing the solenoid of sPHENIX- an upcoming experiment at the RHIC in BNL for the EIC [15]. This chapter discusses a detailed outline of a potential general purpose detector, which would be able to address the physics goals at EIC, making use of several parts of the sPHENIX detector and upgrading some of them. We focus on the EIC-sPHENIX detector in particular as we have access to a full detector simulation of sPHENIX which is modified for EIC, and Stony Brook University is a part of the PHENIX/sPHENIX collaboration.

3.1 EIC-sPHENIX

The EIC detector design reflecting the use of sPHENIX solenoid and refurbishing several other components of sPHENIX goes by a working name "EIC-sPHENIX". The following figure (Figure 3.2) illustrates the EIC-sPHENIX reference design discussed in the chapter and throughout the thesis.

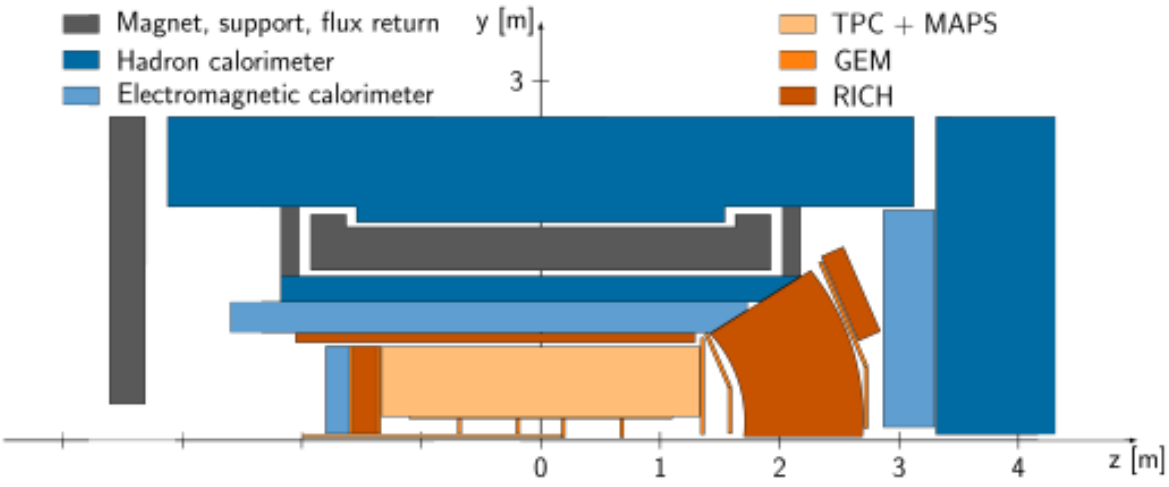

Figure 3.2: EIC-sPHENIX central detector reference design

This detector design uses sPHENIX super-conducting solenoid of 1.5T field with extended coils on both the ends assuring field uniformity, barrel tracking and forward tracking. Further calorimetry and tracking will be implemented in both positive and negative pseudorapidities, and detectors for particle identification (PID) in central, postive and negative pseudorapidities. The sPHENIX solenoid - BaBar has a 3m diameter superconducting coil extending upto

3.5m. Longer tracks and field uniformity improve momentum resolution for high momentum tracks. There is a charged particle tracking setup covering -4 to +4 pseudorapidities.

3.1.1 Components of EIC-sPHENIX

This section discusses some of the main components of the EIC-sPHENIX general purpose detector. The following table gives the information on detector coverage with respect to the pseudorapidities.

Table 3.1: Detector coverage of EIC-sPHENIX reference design

Detector	pseudorapidity	Type
TPC + MAPS + GEM	(-4, 4)	Tracking
barrel EMCAL	(-1.55, 1.24)	Calorimetry
barrel inner HCAL	(-1.1, 1.1)	Calorimetry
barrel outer HCAL	(-1.1, 1.1)	Calorimetry
e-side EMCAL	(-4, -1.55)	Calorimetry
h-side EMCAL	(1.24, 4)	Calorimetry
h-side HCAL	(1.24, 4)	Calorimetry
DIRC	(-1.4, 1.24)	PID
gas RICH	(1.24, 3.95)	PID
h-side mRICH	(1.10, 1.85)	PID
e-side mRICH	(-3.9, -1.4)	PID

Vertex Tracker : The sPHENIX vertex tracker extends over the η range $|\eta| \leq 1.9 - 2.4$ consisting of three layers of pixel tracker called MAPS.

Central Tracking: The Time Projection Chamber (TPC) is the main component in the sPHENIX tracking system which covers a volume extending radially from 20-80 cm and η range from -1.1 $< \eta <$ +1.1. The overall central tracking at EIC-sPHENIX covers all of $-4 < \eta < +4$ with the forward and backward Gas Electron Multiplier (GEM) detectors. In the positive pseudorapidities there are two GEM disks, FGEM0 and FGEM1 at $z = 20$cm and $z = 70$cm respectively which connect to the vertex, vertex tracker and TPC, and three GEM stations each at $z = 140, 160$ and 270 cm away from the nominal collision vertex. These three GEM stations play an important role in momentum measurements.

In the electron going direction at negative pseudorapidities, there are two GEM disks each at $z = -20$ and -70cm, and two GEM stations at $z = -140$ and -160 cm away from the collision point. Due to the limited number of hit points, tracking is poor in the most backward angles and hence poor resolution for momentum reconstruction for particles going in that region.

Electromagnetic Calorimetry: The proposed EIC-sPHENIX design has three major electromagnetic calorimeters one each in the central, forward (hadron-going) and backward (electron-going) directions. As the scattered electron's properties are very significant for the event kinematic reconstruction, the calorimeter present in the negative pseudorapidity - the Electron Electromagnetic Calorimeter (EEMC) has better resolution. It is a crystal calorimeter made of 5000 crystals, with 4x4 Si-PM readouts. A lot of R&D studies has been involved in making scintillating glass/ceramics in order to improve resolution.
The Central Electromagnetic Calorimeter (CEMC) covers a pseudorapidity range $-1.1 < \eta < +1.1$. Extending radially from $r = 90$cm, this calorimeter has 24,596 towers that are read out via silicon multipliers. One of the modifications which can be made to the existing sPHENIX setup is to cover the gap between EEMC and CEMC by extending the CEMC to the electron-going direction.
In the positive pseudorapidities, covering η from $1.24 < \eta < 4$ is the Forward Electromagnetic Calorimeter (FEMC). The CEMC can also be extended forward so as to cover the gap between $1.1 < \eta < 1.24$ which would provide full EMCAL coverage in conjunction with FEMC. Reusing the PHENIX PbSc sampling calorimeter as FEMC is a feasible option.

Hadronic Calorimetry: The hadronic calorimetry at EIC-sPHENIX prospective design involves a forward, inner and outer calorimeters. (Refer the Table 3.1). The forward hadronic calorimeter (FHCAL) is quite important for the forward jet reconstruction as well as for the DIS diffractive events. The inner and outer HCal are essential as they play a significant role in the flux return of the superconducting solenoid. The FHCAL is placed approximately 3.5m away from the interaction point and the design is similar to that of the HCal in the STAR detector.

Particle Identification: One of the most important tasks of a detector system is to

be capable of identifying particles. The major phenomenon we rely on for particle identification is the Cherenkov radiation. There are several detectors which utilise this to identify particles and help in the event reconstruction. The main detectors which help in the particle identification at the EIC-sPHENIX are DIRC (Detection of Internally Reflected Cherenkov light) and, gas and aerogel RICH (Ring Imaging Cherenkov) detectors.
DIRC detector extends over an η range of -1.4 $< \eta <$ +1.24 and plays a significant role in k/π separation. The DIRC works on pinhole focusing which is a method by which the Cherenkov ring image is focused using spherical mirrors. The gas RICH detector is present in the forward direction from $1.24 < \eta < 3.95$. Modular RICH (mRICH) detectors are present in both electron and hadron going directions. (Refer Table 3.1)

Far Forward Detectors: Specifically in the case of coherent diffractive events where the proton is scattered away intact, as in the case of Deep Virtual Compton Scattering (DVCS) and Deep Virtual Vector meson Production (DVMP), detectors in the far forward regions are important. In the case of e-A collisions, we expect to detect the nuclear remnants after incoherent processes in these far forward detectors. As we will see, detection of the scattered proton is very crucial in the event kinematic reconstruction using Jacquet-Blondel and Double-Angle methods. As these protons scatter off at smaller angles $\leq$ 20 mrad, far-froward detectors are necessary in addition to the central detector system. Following figure (Figure 3.3) shows the proposed far-forward detector design for EIC.

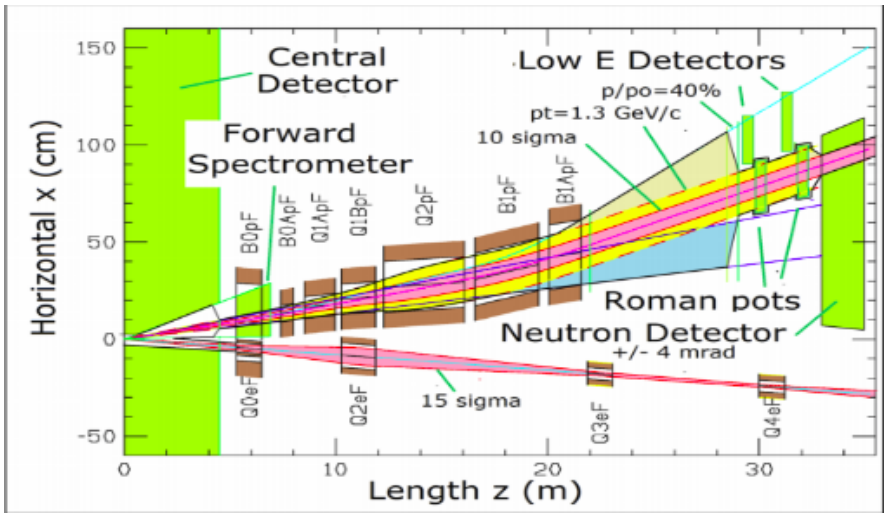

Figure 3.3: Far forward detectors at EIC (adapted from a talk at the -Exploring QCD with light nuclei at EIC- workshop at SBU [29]

The proposed design includes Roman pots which are going to be placed $\simeq$ 30m away from the interaction point. Roman pots are silicon sensors inserted into the beam pipe so as to detect protons scattered at angles $\leq$ 5 mrad. Based on eRHIC pre-CDR [24], it is possible to install two roman pot stations which are approximately 40 metres away from the interaction point (IP) and separated by $\simeq$ 20 cm, with each of these stations having two vertical and horizontal sub-stations in order to have full azimuthal coverage about the beam line. Protons are bent away using magnetic fields and made to hit the roman pots. As their tracks curve in the magnetic dipole field, their momentum can be reconstructed knowing the track curvature. In the case of incoherent diffractive processes involving nuclear breakup, neutrons are also produced in addition to protons and charged nuclei. Since neutrons do not bend with the applied magnetic field, they are typically captured in Zero Degree Calorimeters (ZDC) which are kept far away from the IP at $\simeq$ 40 metres. Hence, one of the ways to distinguish coherent and incoherent diffractive events is to tag them based on the hits on ZDC if any. One of the pressing problems in this scenario is the efficiency of the ZDC as the existing ZDC at BNL has efficiency of approximately 30%.

Having discussed most of the main components of the EIC-sPHENIX, a prospective detector design for EIC, it is pivotal to understand and interpret the data acquisition (DAQ) data rate of each of these sub-systems. The following figure (Figure 3.4) shows the break down of DAQ data rate for $e+p$ collisions in a simulation study using GEANT4 (see Section 3.3), considering only tracking detectors and calorimeters.

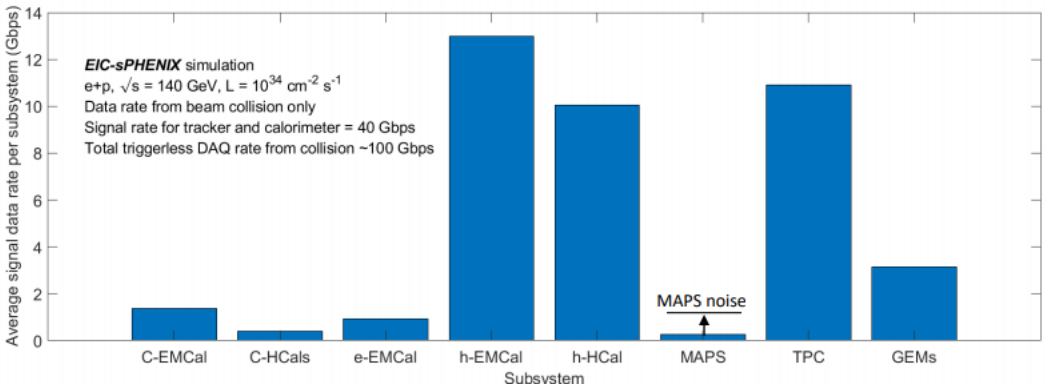

Figure 3.4: DAQ data rate by different detector subsystems at the EIC-sPHENIX [15]

3.2 EIC-smear Simulations

EIC smear is a Monte Carlo (MC) smearing package which performs fast detector smearing to study the resolution effects of the various detector subsystems. The true kinematics of the particles are loaded from the generated output and then modified according to a specified detector description. The eic-smear package is designed so as to analyze in the ROOT framework and, contains classes and functions to facilitate smearing of ROOT trees. The main advantage of using eic-smear as compared to the full GEANT4 detector simulations is its rapid, approximate estimates of detector acceptance and performance on physics observables. Smearing is done using the described resolution making it easier and faster for the code to analyze lots of events in very less time compared to smearing in GEANT4 where the detector properties are specified in detail. Hence, this tool can not be considered as a replacement to the GEANT4, but can be used as an effective method for a quick study on detector acceptance and performance.

During our study on event kinematic reconstruction, the eic-smear package [13] was used to smear the true kinematic variables such as energy and momentum of the MC particles to reflect the performance of an EIC detector based on sPHENIX. The eic-smear package on the repository has a tracking system extending from $-4 < \eta < +4$ and, a resolution is specified by which the total momentum of the particles is smeared as a function of their scattering angle. The various electromagnetic and hadronic calorimeters are specified acceptances as given in the Setting 1 of the proposed EIC-sPHENIX- which is the ideal case where there are no gaps between the electromagnetic calorimeters (See Table 5.1) [19]. In addition, Roman pots were added to the fast simulation assuming different acceptances to analyze the performance in tracking the outgoing proton in the case of coherent ep collisions. In the case of incoherent processes, $e - Au$ breakup events were generated using Sartre and ZDC was added to give an account of the number of neutrons per event that are expected to hit this far forward calorimeter. See Chapter 5 on Event Kinematic Reconstruction to get a detailed view of the analysis.

3.3 GEANT4 Simulations

This section summarizes how the EIC-sPHENIX detector is implemented in a simulation kit with specified acceptances and resolutions for each detector subsystems. Following is

the display output of the full GEANT4 setup (this is being modified for better simulation studies for the upcoming EIC *Yellow Report*).

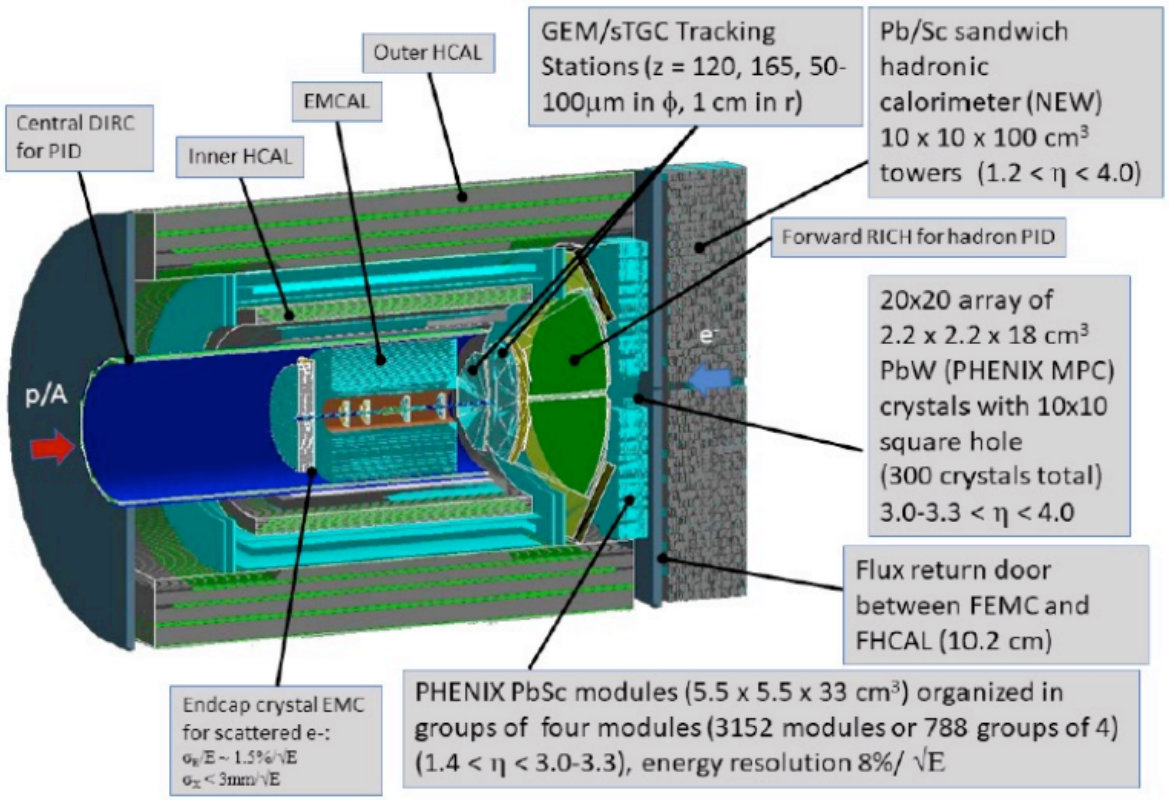

Figure 3.5: Central Detector of the EIC-sPHENIX in GEANT4

As discussed in Section 3.1, the main components of the EIC-sPHENIX, such as the ones which will be reused after the sPHENIX experiment and, the ones which are going to be modified, are implemented (with approximations) in the Fun4AllEIC-sPHENIX code. The tracking system ($-4 < \eta < +4$) is the same as the one implemented within the sPHENIX GEANT4 framework including the TPC, vertex tracker (MAPS), GEMs in electrons going (EGEMs) and hadron going forward (FGEMs) directions.The inner and outer HCALs, EEMC, FEMC and CEMC are also implemented with specific energy resolution. For particle identification, a large central DIRC, forward RICH detectors are implemented leaving a space in the negative rapidity for the aerogel RICH detector.

For my event kinematic reconstruction studies, Sartre MC output was run through the set up (as shown in the Figure 3.5), and using the calorimeter cluster, PID, and tracking informa-

tion, particles falling in the specified acceptance of η were reconstructed. Later, these kinematic properties of identified particles were used to reconstruct the event kinematics using the three different methods (See Chapter 5 for more details). The scattered proton/nucleus cannot be reconstructed with the existing setup as it has only the central detector. In fact, a separate framework called *EIC-Root*[14] incorporates the far forward detector system, as in Figure 3.3. Thus, integrating both the central detector and far forward detectors is one of the biggest demands at the moment for a detailed study on analyzing detector performance in order to get a more realistic picture.

Chapter 4

Decay Angular Distribution

Electron-Ion Collider is an upcoming machine to unveil the secrets of the strong force in nature. It would consist of two intersecting accelerators- electrons and protons/ heavy nuclei which are steered into head-on collisions. In an EIC, the structure of the hadron (which can be a proton or a heavy nucleus) is probed via the process of Deep Inelastic Scattering.

Diffractive Deep Inelastic Scattering (DDIS) processes are important as they are sensitive to geometric structure of hadrons, and are effective in understanding the gluon spatial distribution inside nuclei, and also the saturation phenomena. These processes are, theoretically, distinguished by the colorless gluon exchange between the virtual photon and participating hadron, and experimentally by the presence of a rapidity gap. In a coherent diffractive process the nucleus stays intact whereas in the incoherent events, nucleus breaks up into fragments which would need far forward detectors to get detected. In a Diffractive Vector Meson Production (DVMP), the vector meson is the only new final state.

Sartre [20] is an event generator for exclusive diffractive vector meson production and Deeply Virtual Compton Scattering in ep and eA collisions based on the dipole model. It describes the process,

$$e + p \rightarrow e' + p' + V$$
$$e + A \rightarrow e' + A' + V$$

where V = J/ψ , ϕ, ρ, γ.

Using Sartre,

$$e + Au \rightarrow e' + Au' + J/\psi$$

events were generated by specifying J/ψ decay to e^+ and e^-. Event kinematic reconstruction studies were done at the generator level, later convinced by the dominance of the Scattered Electron method in resolution as compared to the Jacquet Blondel and the Double Angle methods. Hence, further studies directed to investigate how precisely the scattered electron's energy and scattering angle can be measured. One of the posing questions was the decay angular distribution of the J/ψ, as it decays to e^+e^- pair, and the chances of misidentifying the scattered electron can not be neglected.

4.1 Decay Angular Distribution of J/ψ

It has been observed that [22] the polarization of the virtual photon accounts for the decay angular distribution of the VM. At lower Q^2, photons are transversely polarized to the beam direction; they can be decomposed in a way that half a fraction of them are right handed and the rest half left handed. In this case, the vector meson retains photon spin state and the decay angular distribution comes from the Clebsch Gordon coefficients and spherical harmonics. But the situation gets complicated at higher Q^2, as the photon starts being longitudinally polarized, in addition, along the beam direction. In the following diagram (Figure 4.1), Φ and ϕ are the angles made by the VM production plane with the electron scattering plane and the VM decay plane, respectively, in the hadron centre-of-mass frame, while θ is the polar angle of the positive decay product in the VM rest frame - measured relative to the VM direction in the hadronic COM frame.

Following the formalism used in [22], the decay angular distribution can be expressed in terms of 15 spin density matrix elements which correspond to different bilinear combinations of the helicity amplitudes of the particular vector meson production.

-s-channel helicity conservation (SCHC)

According to the SCHC, the helicity of the virtual photon is retained by the vector meson and the helicity of the nucleus/proton is unchanged.

Following the SCHC approximation, Natural Parity Exchange (NPE) and certain other approximations, the different helicity amplitudes can be related and, most of the matrix ele-

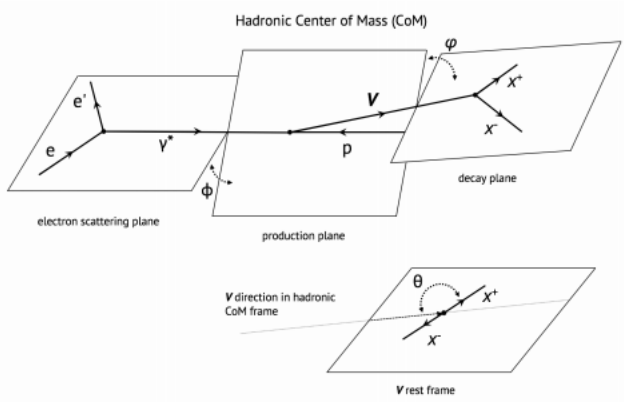

Figure 4.1: A schematic diagram describing the process $e + p \rightarrow e' + V + p'$, and relevant angles used in this study [21]

ments vanish except for r_{00}^{04}. The matrix elements can be measured as the projections of the decay angular distribution onto orthogonal trigonometric functions of these angles θ, ϕ and Φ, as shown in Figure 4.1. We can thus obtain information about the polarization of the virtual photon based on the measurements of the spin density matrix elements, using SCHC as a first order approximation. After integrating over the angles ϕ and Φ, the differential cross section can be weighed w.r.t the cosine of the angle θ and the decay angular distribution takes the form as follows (for VMs like J/ψ which decays to spin-1/2 leptons)

$$\frac{dN}{dcos\theta} = \Omega(cos\theta) = \frac{3}{8\pi}(1 + r_{00}^{04} + (1 - 3r_{00}^{04})cos^2\theta) \tag{4.1}$$

where θ is the angle, in the J/ψ rest frame, between the positive decay product e^+ and J/ψ direction in the hadronic COM frame. (See Figure 4.2.) In the case of SCHC, the matrix element r_{00}^{04} provides a direct relation with the ratio of cross-sections of vector meson production by longitudinal and transversely polarized virtual photon as follows,

$$R = \frac{1}{\epsilon}\frac{r_{00}^{04}}{1 - r_{00}^{04}} \tag{4.2}$$

where ϵ is the parameter describing the polarization of the virtual photon given by (for large $\sqrt{s}$)

$$\epsilon \simeq \frac{1 - y}{1 - y + y^2/2} \tag{4.3}$$

As SCHC violating amplitudes are small compared to the helicity conserving ones, equation (4.2) is used to estimate the value of r_{00}^{04} assuming SCHC. Under SCHC approximation we

also find that the azimuthal angle ϕ assumes a uniform distribution as the spin matrix element r^{04}_{1-1} vanishes. There are two ways to get the value of R: 1) using the 3-fold cross-section ratio from Sartre or 2) using the equation below [21],

$$R_V(W^2, Q^2) = \frac{\sigma_{L,\gamma^* p \to Vp}}{\sigma_{T,\gamma^* p \to Vp}} = \frac{(Q^2+m^2_{V,T})^2}{m^4_{V,T}} \zeta^2_V \left[\frac{\pi}{2} \frac{m^2_{V,L}}{Q^2} - \frac{m^3_{V,L}}{\sqrt{Q^2}(Q^2+m^2_{V,L})} - \frac{m^2_{V,L}}{Q^2} arctan(\frac{m_{V,L}}{\sqrt{Q^2}}) \right]^2$$

where $m_{V,L}$ and $m_{V,T}$ are modified pole masses, and ζ_V is the ratio of imaginary forward scattering cross-sections for longitudinally and transversely polarized VMs. These parameter

Mesons	$m^2_{V,L}$	$m^2_{V,T}$	ζ_V
ρ	$0.71\ m^2_\rho$	$0.68\ m^2_\rho$	1.06
ϕ	$0.57\ m^2_\phi$	$0.41\ m^2_\phi$	0.9
J/ψ	$0.6\ m^2_{J/\psi}$	$0.6\ m^2_{J/\psi}$	1

Table 4.1: Table showing the pole masses and ζ_V values for different mesons

values were determined by fitting to HERA data for lighter mesons, but at EIC we are interested in heavier mesons like J/ψ (Refer Table 4.1). For J/ψ, certain approximations were made to get the parameter values. The decay angular distribution is plotted as a function of cosθ in J/ψ rest frame and in the lab frame (see Figure 4.2). As we expect, the

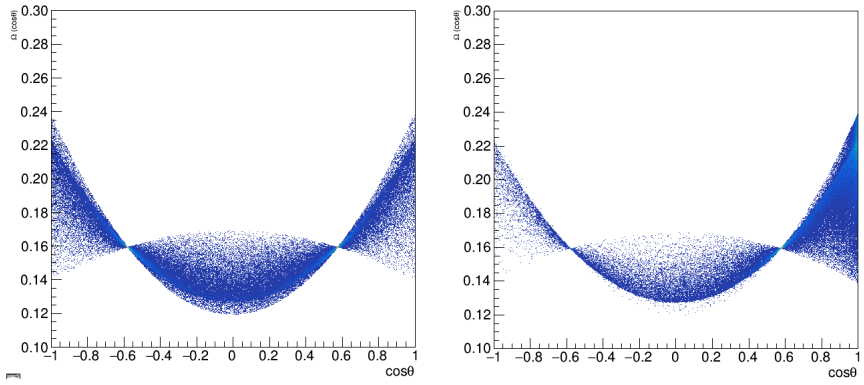

Figure 4.2: Decay angular distribution plotted as a function of cosθ ((a) in VM rest frame (b) in lab frame)

spread shifts to the right in the lab frame implying the daughters move closer to J/ψ. Now the motive is to boost back to the lab frame, so the modified decay angle can be compared with the one given by Sartre.

4.1.1 Analysis and Interpretations

The R distribution is found to be consistent with the equation above as well as using the ratio given by Sartre (Figure 4.3). The dependence of R on event W and t can be neglected but, on Q^2 is quite significant. This is the reason why we were able to get consistent results after substituting the formula above with the triple differential cross-section ratio given by Sartre, ie, $\frac{d\sigma}{dtdQ^2dW^2}$.

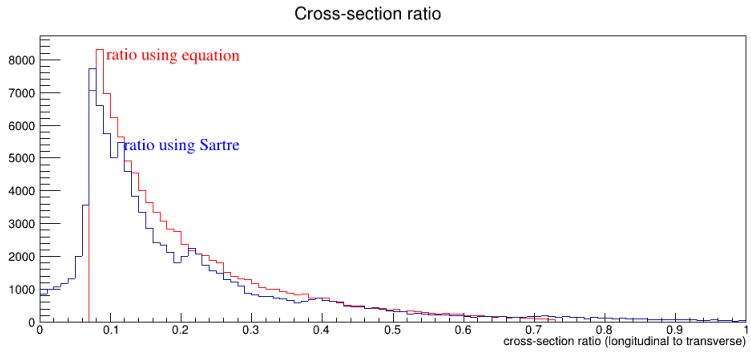

Figure 4.3: Longitudinal to transverse cross-section ratio

The angle which is defined in the rest frame of the VM can be boosted back to the lab frame applying the weights given by the distribution in Equation (4.1). It is observed that the VM and its daughter would move closer. A comparison plot of the angular distribution after applying weight given by the equation (4.1) and the one given by Sartre kinematics is studied. The distribution is similar keeping the detector acceptances of the VM daughter unchanged. Therefore, this detector acceptance range can be plotted along with that of the scattered electron to see if these two electrons overlap in the space.They are well separated in ϕ but, overlap in certain η regimes. Using the proposed detector acceptance ranges of the sPHENIX (as per the LOI 2018 considering all the 6 different settings), it is observed that detector acceptances of both the scattered electron and the VM daughter electron overlap in the EEMC region. A projection to the detector can be made to see the physical separation of them when they hit the detector. It is observed that in most of the cases these two are well separated ($\simeq$ cm), implying less chances of misconceiving the measurements of the scattered electron, which is our primary goal so as to accurately reconstruct the event kinematics.

4.2 Implementing Source Code

Following is our method of approach:

- We boosted the VM from the lab frame to the hadronic COM frame. This gives us the VM 4-vector in the COM frame, with the Cartesian coordinate system in the COM frame consist with that defined in the lab frame.
- In the VM rest frame, we generated the VM decay products using a uniform distribution over a sphere. This gives us 4-vectors for the VM daughters in the VM rest frame, again with the Cartesian coordinate system consistent with the lab frame.
- In the VM rest frame, the angle between one of the VM daughters and the VM momentum direction in the hadronic COM frame is calculated. This angle is used to provide the event weight. The distribution of $\frac{dN}{dcos\theta}$ as a function of $cos\theta$ in the VM rest frame (See Figure 4.2 (a)) is plotted.
- The VM daughters are first boosted to the hadronic COM frame and, then to the lab frame to obtain the VM daughter 4-vectors in the lab frame. (We could also boost the daughters from the VM rest frame directly to the lab frame - by using the VM 4-vector in the lab frame.) We then calculated the θ between one of the daughters and the VM in the lab frame to get the distribution in the lab frame (See Figure 4.2 (b)).

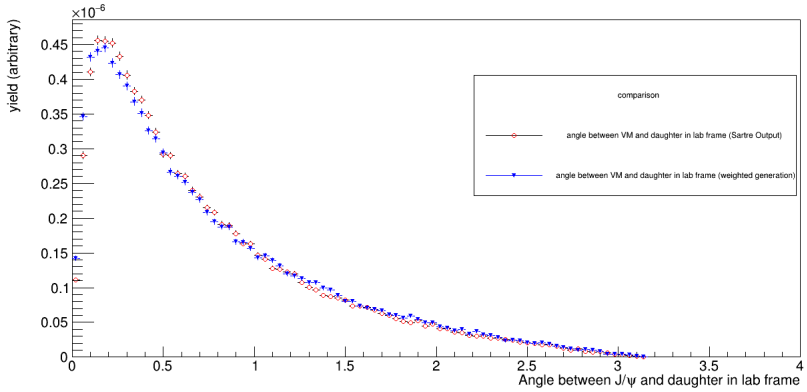

Figure 4.4: Angle between VM and its daughter (after normalization)

- The θ calculated above is then weighted and compared with the distribution given by Sartre kinematics to get the following (see Figure 4.4). Since the decay angular

distribution should not affect the 3-fold cross section, we normalize the distribution by dividing by the sum over all event weights.

- As a verification, the angular distribution obtained in the step above without applying weight is found to be consistent with that given by the default Sartre output.

Chapter 5

Event Kinematic Reconstruction Studies

In Section 2.1, we discussed several kinematic variables associated with a Deep Inelastic Scattering process. Reconstructing these quantities is crucial not only to measure the structure functions, but also getting a good grasp of these variables help in understanding the underlying physics process. This chapter discusses the three complementary event kinematic reconstruction methods - the Scattered Electron Method, Jacquet Blondel Method and the Double Angle Method.

In the Scattered Electron Method, we would require the scattered electron's energy and scattering angle to reconstruct the entire event kinematics. Hence, this method is feasible in inclusive, semi-inclusive and, exclusive processes as long as the scattered electron is detected. In the Double Angle Method, we would need to know the scattering angles of the scattered electron as well the hadronic final state. In case all information about the scattered electron is missed, the Jacquet-Blondel Method gives a fair way for the reconstruction where only the information such as the effective scattering angle and energy of the hadronic final state are required. In this chapter, an elaborate discussion and comparison of these three methods implemented on exclusive diffractive processes, both at generator level and after running through the detector is being made followed by a brief discussion on different kinematic regimes at EIC using various phase space plots.

5.1 Kinematic Reconstruction Methods

In a deep inelastic scattering process, the electron couples with the proton/nucleus via a photon or gauge boson such as Z or W and probes the proton/nucleus. Depending on the detected final state, the process can be neutral current (NC) - when the final state detected is electron, or charged current (CC) - when the final state detected is a neutrino.
Let us consider the process of diffractive deep inelastic scattering process of J/ψ production as shown in the figure below (Figure 5.1). This diagram can be best described using the

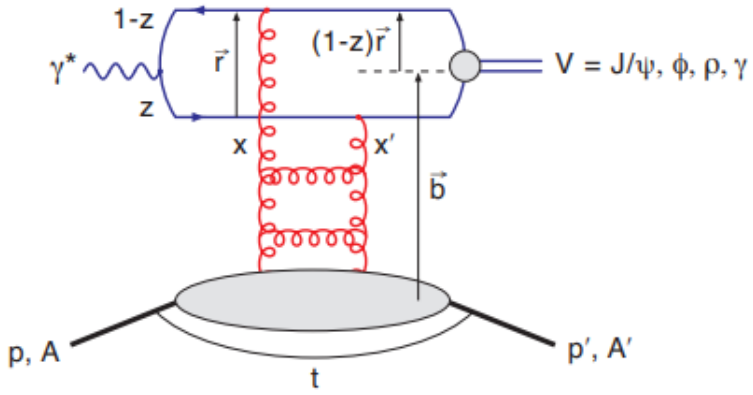

Figure 5.1: A schematic diagram showing DVMP in dipole picture [20] Here r is the dipole length and z is the fraction of virtual photon's momentum carried by the vector meson

dipole model. In the dipole picture, the virtual photon fluctuates to give $c\bar{c}$ - the *dipole*, before the actual scattering takes place. It is this produced dipole which later scatters off the target proton/nucleus. The splitting of $\gamma^* \rightarrow q\bar{q}$ is described by the virtual photon wave function Ψ. In the case of vector meson production as shown in the figure (Figure 5.1), the dipole transitions to a vector meson, which in our studies is J/ψ, and the transition is described by wave function $\Psi_{J/\psi}$.
Let us consider the kinematics of an exclusive diffractive process.
The four momenta of the initial and final state electron are denoted by k and k', and that of the initial proton and final state hadron (hadronic system in case of inclusive scattering) are p and p'. We can write E_e and E'_e to represent the incoming energy of the electron and the energy after scattering, respectively. Considering E_p to be the incoming energy of the proton/nucleus, let us express the four momenta of the different particles as follows.

$$k = \Big(0, 0, -E_e, E_e\Big) \qquad p = \Big(0, 0, E_p, E_p\Big)$$
$$k' = \Big(E'_e sin\theta_e cos\phi_e, E'_e sin\theta_e sin\phi_e, E'_e cos\theta_e, E'_e\Big) \qquad p' = \Big(\Sigma_h P_x^h, \Sigma_h P_y^h, \Sigma_h P_z^h, \Sigma_h E^h\Big)$$

Here θ_e and ϕ_e are the polar and azimuthal angles of the scattered electron, where θ is measured with respect to the incoming proton beam. The notation Σ_h indicates the summation over all the hadronic final states. In case the proton/nucleus does not break up and gets detected, as in coherent exclusive scattering, the summation can be ignored and the information of the outgoing proton is considered for the calculation. Hence, hadronic final state consists of everything other than the leptonic final state. When both the hadronic and leptonic final states are measured, we will have following four independent quantities, E'_e, θ_e, $(p_x^2 + p_y^2)_h$ and $(E - p_z)_h$ with which we find several ways to reconstruct event kinematics. The following figure (Figure 5.2) illustrates the important kinematic quantities that will be used in the reconstruction.

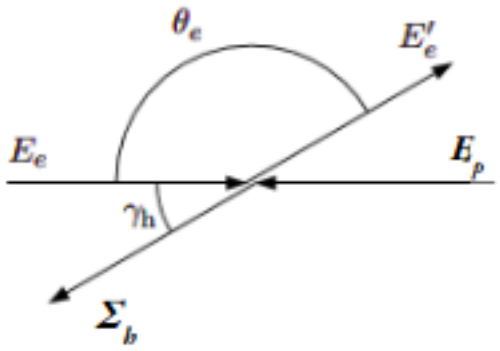

Figure 5.2: DIS interaction showing the important kinematic variables used in the different reconstruction methods (adapted from [30])

Scattered Electron Method:- In this method, we reconstruct variables x, Q^2, y using the energy and angle of the scattered electron.

$$\begin{aligned} y_{el} &= 1 - \frac{E'_e}{E_e} sin^2 \frac{\theta_e}{2} \\ Q^2_{el} &= 2E'_e E_e (1 + cos\theta_e) \\ x_{el} &= \frac{E'_e (1 + cos\theta_e)}{2yE_p} \end{aligned} \tag{5.1}$$

and the inverse relations can be written as,

$$\begin{aligned} E'_e &= (1 - y_{el})E_e + xyE_p \\ cos\theta_e &= \frac{\big(xyE_p - (1-y)E_e\big)}{\big(xyE_p + (1-y)E_e\big)} \\ E'^2_e sin^2\theta_e &= 4xy(1-y)E_eE_p \end{aligned} \tag{5.2}$$

It is evident that this method requires good reconstruction of energy and angle of the scattered electron. When this method was implemented on the diffractive events at generator level (using Sartre kinematics), we observe that the reconstructed quantities are very well correlated with the true values. See Figure 5.3. Hence, in order to reconstruct event kine-

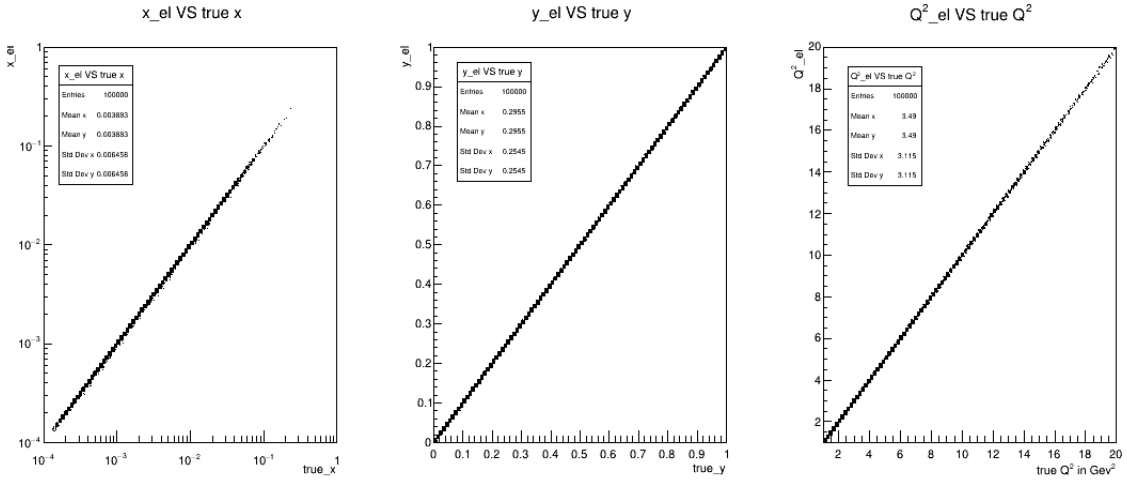

Figure 5.3: Scattered Electron method reconstructed x, y and Q^2 plotted against the respective true values at generator level

matics accurately, the calorimeters which get the scattered electron hits have to be efficient and, made to improve resolution.

Jacquet Blondel Method:- This method comes into play when the electron gets undetected or, in the case of CC events where a final state neutrino is formed. In this method, the kinematic variables are reconstructed entirely using the hadronic energy flow. It turns out that,

$$q = (k - k') = (p - p')$$

where q is the four momentum transferred to the virtual photon in Figure 2.1, and we know from equation (2.7) that,

$$y = \frac{p.q}{p.k}$$

Thus, we can write,

$$\begin{aligned} y_{JB} &= \frac{\Sigma_h (E - p_z)_h}{2E_e} \\ Q^2_{JB} &= \frac{(\Sigma_h p_{x,h})^2 + (\Sigma_h p_{y,h})^2}{1 - y_{JB}} \\ x_{JB} &= \frac{Q^2_{JB}}{y_{JB} s} \end{aligned} \tag{5.3}$$

where s is the centre of mass energy of the system. Following figure (Figure 5.4) shows the reconstruction of the above variables using this method at a generator level.

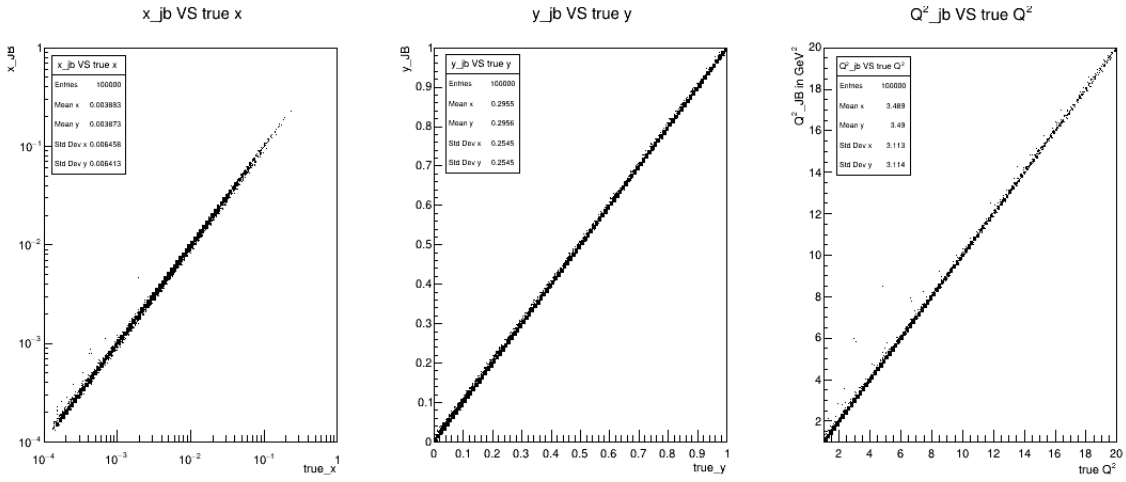

Figure 5.4: Jacquet-Blondel method reconstructed x, y and Q^2 plotted against the respective true values at generator level

Though we have not included any detector smearing, a very close observation tells us that this method has relatively poor resolution, especially in x and Q^2 as compared to the electron method. One of the key points to keep in mind is the assumption this method rests on - the total transverse momentum of the protons or particles going through the beam hole, hence not detected in the proton direction, as well as that of the electrons going through the beam hole escaping detection in the electron going direction, can be neglected.

Double Angle Method:- In a combined method of this kind, we use measured properties of both the hadronic and leptonic final states, hence call this a mixed method; and these properties are the scattering angle of the electron (θ_e) and, the effective angle of the hadronic final state (γ_h - also known as the scattering angle of the struck quark in naive parton model) (See Figure 5.2), hence call this the Double Angle Method. The angle γ_h characterizes the

longitudinal and transverse momentum flow of the hadronic system, and can be expressed as,

$$cos\gamma_h = \frac{(\Sigma_h p_{x,h})^2 + (\Sigma_h p_{y,h})^2 - (\Sigma_h (E_h - p_{z,h}))^2}{(\Sigma_h p_{x,h})^2 + (\Sigma_h p_{y,h})^2 + (\Sigma_h (E_h - p_{z,h}))^2} \tag{5.4}$$

The kinematic variables can then be written in terms of θ_e and γ_h as following,

$$\begin{aligned} Q^2_{DA} &= \frac{4E_e^2 sin\gamma_h (1 + cos\theta_e)}{sin\gamma_h + sin\theta_e - sin(\gamma_h + \theta_e)} \\ x_{DA} &= \Big(\frac{E_e}{E_p}\Big) \frac{sin\gamma_h + sin\theta_e + sin(\gamma_h + \theta_e)}{sin\gamma_h + sin\theta_e - sin(\gamma_h + \theta_e)} \\ y_{DA} &= \frac{Q^2_{DA}}{x_{DA} s} \end{aligned} \tag{5.5}$$

where s is the centre of mass energy of the system as before. One of the main advantages of using this method is that it does not rely on any exact energy measurements, instead the ratio of energies; hence insensitive to energy scale. In first order, neither the calibration uncertainties nor the energy loss before the calorimeter plays a significant role. The following figure (Figure 5.5) shows the correlation between true and reconstructed kinematic quantities using the Double Angle Method.

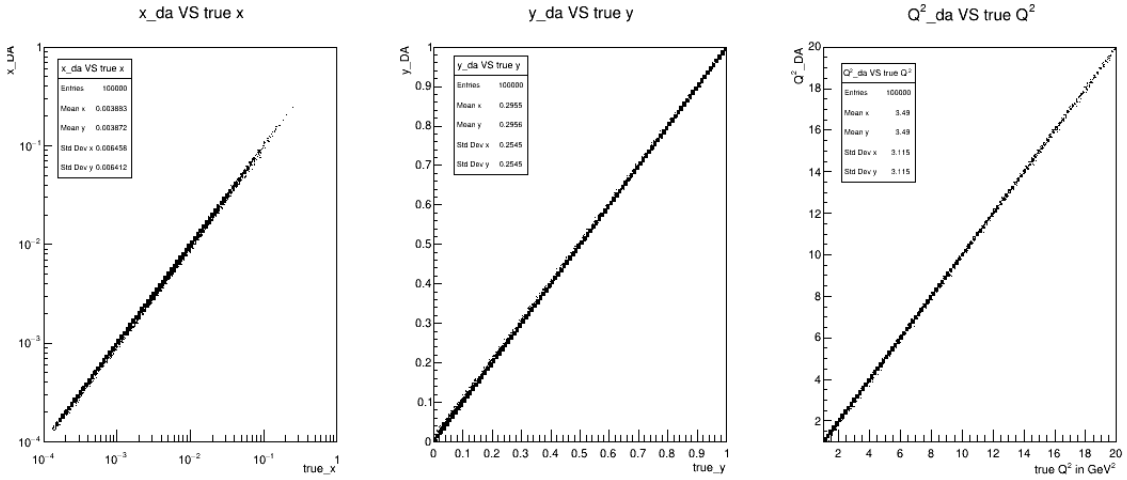

Figure 5.5: Double Angle method reconstructed x, y and Q^2 plotted against the respective true values at generator level

To summarize the generator level comparisons of all the three different kinematic reconstruction methods, see the figure below (Figure 5.6).
As it is evident, the reconstruction using scattered electron method stands too close to the

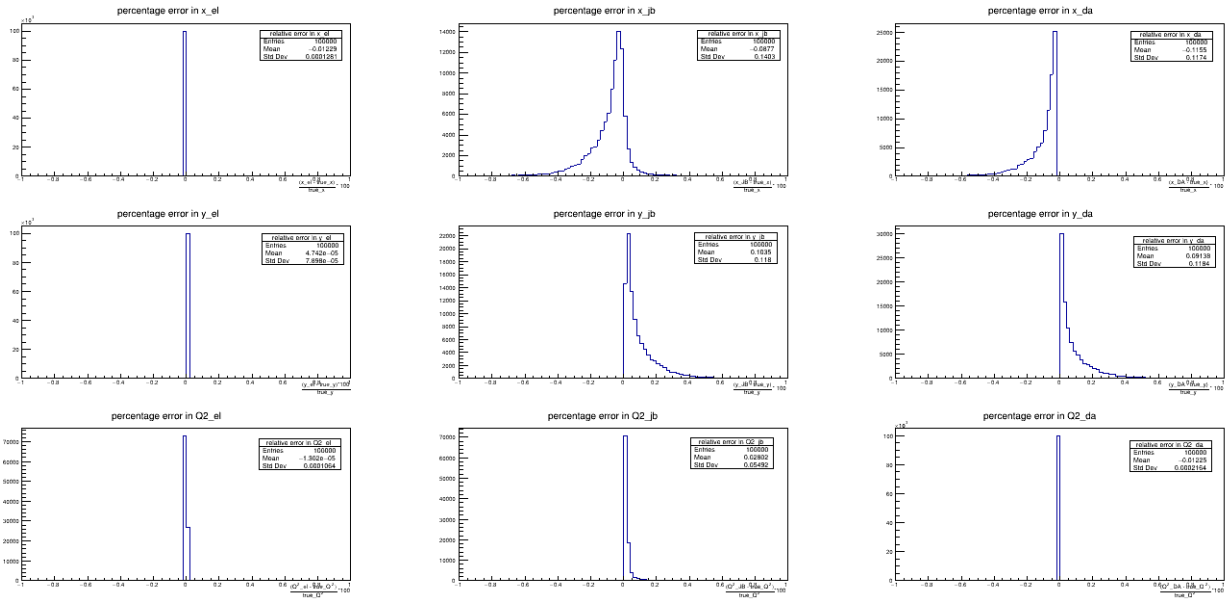

Figure 5.6: The resolution at generator level in x,y and Q^2 (each column respectively) for Scattered Electron, JB and DA methods (each row respectively) for exclusive diffractive J/ψ production at fixed centre-of-mass energy. Here, the reconstruction using JB and DA methods included the outgoing proton in the hadronic final state along with the VM.

true values as compared to other methods in all the three reconstructed variables x, Q^2, and y. The reconstructed y is slightly over estimated in both Jacquet Blondel and Double Angle methods. The x reconstructed using Jacquet Blondel method is poor among all while it is under estimated in the Double Angle method. More or less all the three methods agree fairly on the reconstructed Q^2 values. The resolution in JB and DA methods improve significantly after including the outgoing proton in the hadronic final state along with the vector meson, rather than the vector meson alone. But, all these conclusions are based on the generator level simulations. Following sections of the chapter give a detailed analysis on these methods after considering detector uncertainties and resolutions - smeared using the package eic-smear and full GEANT4 detector simulations.

5.2 Reconstruction using EIC-smear

The same Sartre events were passed through the EIC-smear package to do the event kinematic reconstruction using the same methods. Before discussing the resolutions in x,y and Q^2, we will look at the different settings of EIC-sPHENIX as mentioned in Section 3.2. The

following table (Table 5.1) is taken from the LOI 2018 [19].

Table 5.1: Detector acceptances for different EIC-sPHENIX scenarios as per LOI 2018

	Scenario 0 (sPHENIX)		Scenario 1		Scenario 2		Scenario 3		Scenario 4		Scenario 5	
Detector	eta_min	eta_max	eta_min	eta_max	eta_min	eta_max	eta_min	eta_max	eta_min	eta_max	eta_min	eta_max
TPC	-1.1	1.1	-1.1	1.1	-1.1	1.1	-1.1	1.1	-1.1	1.1	-1.1	1.1
Tracking	-1.1	1.1	-4	4	-4	4	-4	4	-4	4	-4	4
EEMC	--	--	-4	-1.55	-4	-1.55	-4	-1.55	-4	-1.55	-4	-1.434
CEMC	-1.1	1.1	-1.55	1.242	-1.55	1.1	-1.1	1.242	-1.1	1.1	-1.1	1.1
FEMC	--	--	1.242	4	1.45	4	1.242	4	1.45	4	1.45	4
IHCAL	-1.1	1.1	-1.1	1.1	-1.1	1.1	-1.1	1.1	-1.1	1.1	-1.1	1.1
OHCAL	-1.1	1.1	-1.1	1.1	-1.1	1.1	-1.1	1.1	-1.1	1.1	-1.1	1.1
FHCAL	--	--	1.242	5	1.45	5	1.242	5	1.45	5	1.45	5
EPID ('mRICH')	--	---	-4	-1.55	-4	-1.55	-4	-1.55	-4	-1.55	--	--
CPID ('DIRC')	--	--	-1.55	1.242	-1.55	1.242	-1.55	1.242	-1.55	1.242	-1.55	1.242
FPID0 ('RICH')	--	--	1.242	4	1.45	4	1.242	4	1.45	4	1.45	4
FPID1 ('mRICH')	--	--	1.242	1.85	1.45	1.85	1.242	1.85	1.45	1.85	1.45	1.85
FPID2 ('TOF')	--	--	1.85	4	1.85	4	1.85	4	1.85	4	1.85	4

As we see, Setting 1 is the ideal setting where there are no gaps between CEMC and FEMC or CEMC and EEMC. There are continuous tracking and calorimetry detector systems from $-4 < \eta < 4$. In the eic-smear, we have the calorimeters with acceptance ranges given by the Setting 1. The calorimeter energies are smeared as a function of the true energies, and momentum smeared as a function of θ in the acceptance range $-4 < \eta < 4$. With this setup, we can do the reconstruction studies using Scattered Electron, Jacquet Blondel, and Double Angle methods. We have also done the reconstruction using JB and DA methods with and without including proton. As we have discussed in the generator level studies, detecting the proton is crucial. Since the existing set up does not have far forward detector system, we implemented Roman pot at varying distances from the nominal collision point, ie, 30, 40 and 50 metres away from the interaction point to see the effect it has on the efficiency on detecting the protons. Also, referring to the [29] which was presented at a workshop on *Exploring QCD with light nuclei at EIC* at Stony Brook University, a dependence on centre of mass energy, on the resolution of the transverse momentum of protons detected using roman pots, is observed.

Our analysis on varying the roman pot position from the collision point shows that it has no significant effect on the efficiency of roman pots with a particular acceptance. Hence, our further studies were on varying the acceptances of roman pot kept at a fixed position. As mentioned in [15], roman pots are meant to detect protons scattering at angles ≤ 5 mrad. However, we considered different scenarios where the acceptances varied between 2-15 mrad

in differences of 5 mrad, and also the same difference of 5 mrad from 5-25 mrad. From our analysis, we observed that almost 73% of the protons get scattered at angles between 2-10 mrad when roman pot is kept at 40 m away from the collision point. Also, the same figure drops by 63% to just 27 percent of the protons being scattered at angles between 5-15 mrad. This implies that a significant fraction of the protons get scattered at angles between 2-5 mrad. These studies were done using the eic-smear and, were merely a projection of the scattered proton on the roman pots rather than bending the track curve for protons using dipole magnetic fields, in which case the scattering angle is highly correlated with the transverse momentum of the outgoing proton (A detailed study using the full far forward detectors can be done modifying the GEANT4 by incorporating the EIC-Root framework). The following figure (Figure 5.7) shows the reconstruction of x, y and Q^2 using three different methods after smearing the particles using eic-smear.

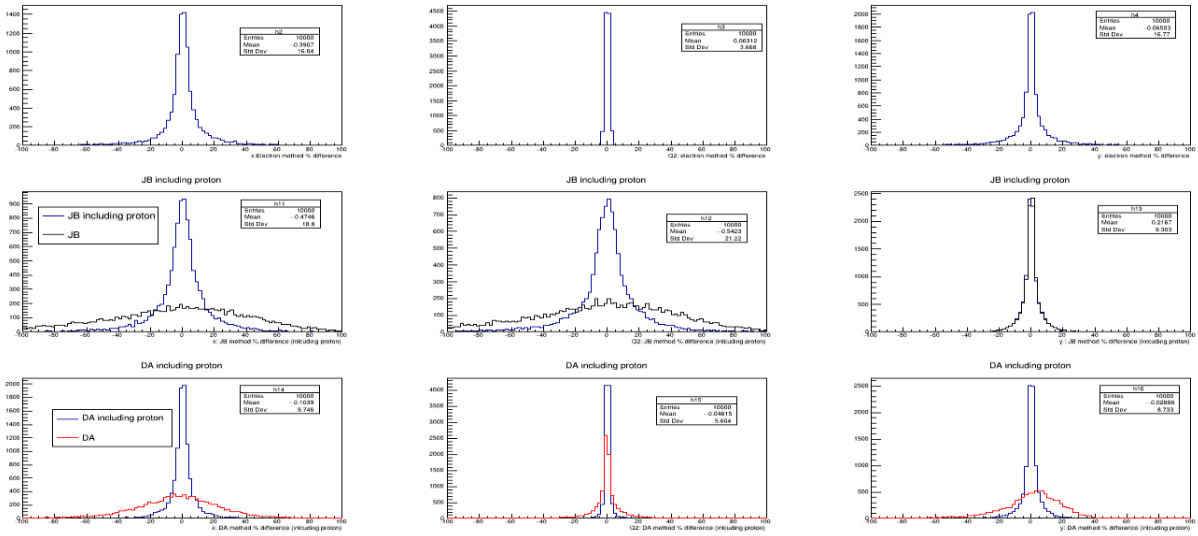

Figure 5.7: Reconstruction of x,y and Q^2 after smearing using eic-smear. The kinematic quantities x, Q^2 and y are shown in each column respectively and, each row corresponds to Scattered electron, JB and DA methods respectively. The blue curve in second row corresponds to reconstruction using JB including the scattered proton in the hadronic final state while the black curve is without, ie, considering the vector meson only. Similarly in the third row, reconstruction done using DA method with proton is shown in blue curve and without proton in red curve.

Another important factor to consider is the position resolution of the roman pots. We tried varying the position resolution, from 100 microns to 10 microns. Following figure (Figure 5.8) shows the impact of improving the position resolution from 100 microns in Figure 5.7 to 10 microns, on the JB and DA methods of event kinematic reconstruction including proton

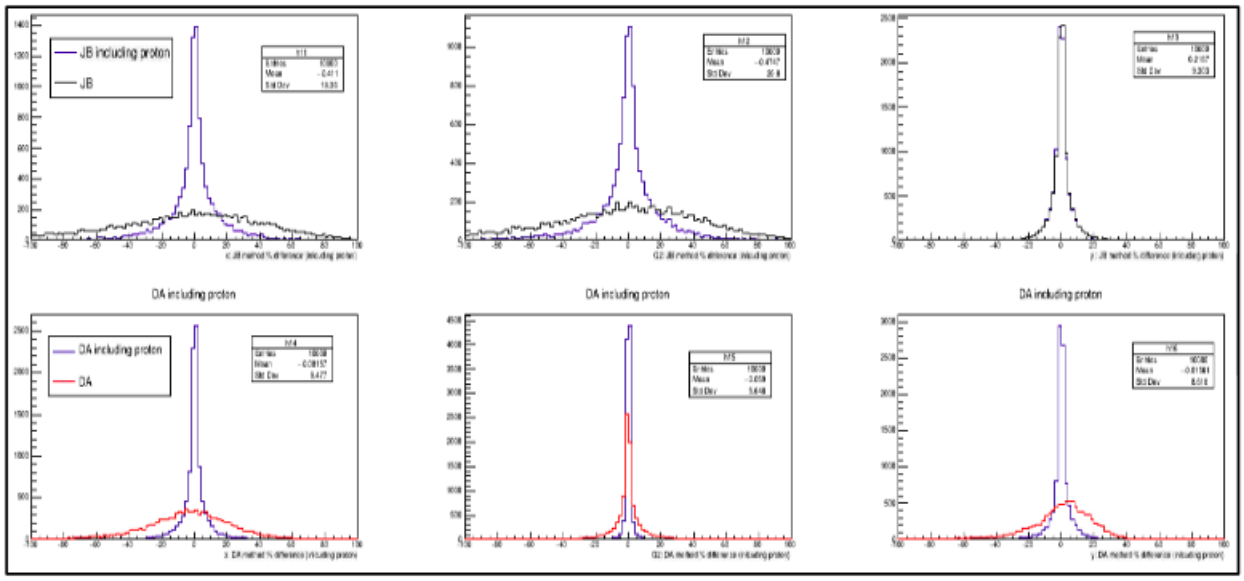

Figure 5.8: Reconstruction of x,y and Q^2 after improving the position resolution of roman pots. The blue curves which correspond to the reconstruction including proton are narrower than those in Figure 5.7.

in the hadronic final state. As we can see, the blue curve in the two rows narrow down giving more accurate reconstruction with higher position resolution, as compared to Figure 5.7. However, 10 micron position resolution is considered an ambitious and expensive demand for EIC.

We have also done the kinematic reconstruction for ep collisions at high Q^2 (since Sartre generates only ep collisions with higher Q^2 ranges), and observed that all the reconstruction methods, in general, gives fairly more accurate results with increasing Q^2.

The following figure (Figure 5.9) shows the reconstruction of eAu events generated at low Q^2. As observed in the generator level studies, eAu reconstruction has better accuracy than ep events, especially in the JB and DA methods. As the final state Au doesn't get detected, reconstruction using JB and DA methods were done considering only vector meson in the hadronic final state.

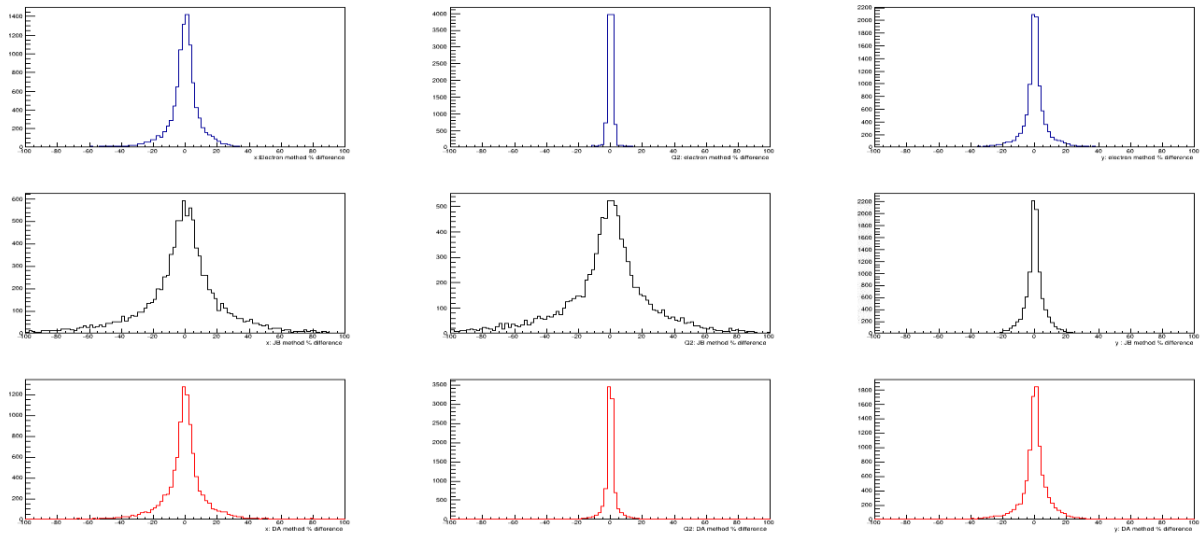

Figure 5.9: x, Q^2 and y reconstruction (each column respectively) using Scattered Electron, JB and DA methods (each row respectively) for eAu collisions. It is observed that JB and DA methods give better accuracy in eAu as compared to ep coherent diffractive processes.

5.3 GEANT4 Detector Simulation Studies

The full GEANT4 detector set-up for EIC-sPHENIX is based on the Setting 1, as shown in Table 5.1. These detector simulations can be used for evaluating the performance of the various detector subsystems at the proposed EIC-sPHENIX, which will be helpful for parameterising these detectors based on GEANT4. Furthermore, these parameterisations can be implemented in various fast simulation packages such as eic-smear. Before discussing the efficiency and performance of the detectors, let us see where the primary electron gets scattered in our diffractive vector meson production processes. The following figure (Figure 5.10) shows the pseudorapidity of scattered electrons in different centre of mass energies. As we see, most of the primary electrons are scattered in the negative pseudorapidities and hence, will be depositing their energies in the EEMC. At lower centre of mass energies, the curve shifts to the right with a significant fraction of the scattered electron falling in the CEMC. But in the EIC, the lower centre of mass energy scenarios are less probable. Hence, the focus of R&D should be on improving the granularity and thereby, resolution of the electromagnetic calorimeter on the electron going side.

One of the other crucial factors is the tracking efficiency in the electron going side. As discussed in Section 3.1.1, there is poor tracking in the electron going direction because of

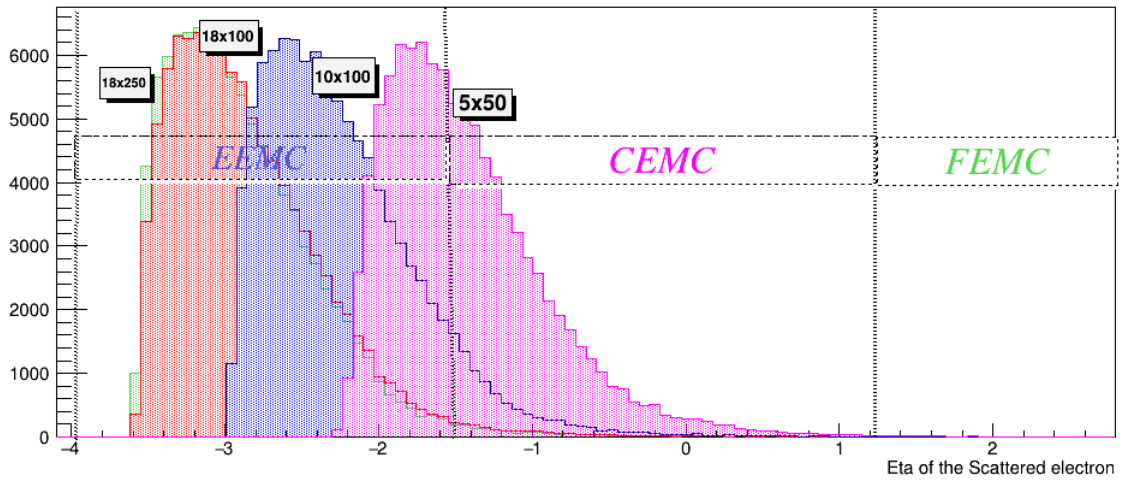

Figure 5.10: Pseudo-rapidity of the scattered electron at different centre of mass energies. The pseudorapidity coverage of different electromagnetic calorimeters is given by the Setting 1 - ideal setting with no gaps.

the less number of GEMs present in that region as compared to the number in the forward region. Tracking system implemented in the GEANT4 too turns out to give poor resolution in the negative pseudorapidities. The reconstruction using Scattered Electron method, as we see in the generator level and the fast simulations with detector smearing, is the most accurate method for event kinematic reconstruction. Hence, tracking the scattered electron, and getting accurate information about the energy deposits in the calorimeter clusters are very crucial in event reconstruction. The following figure (Figure 5.11) shows the efficiency of GEANT4 detector set up as a function of η and momentum. The plot in Figure 5.11 is made such that each box in the 2D histogram gives the efficiency of calorimeters in that particular η and momentum range. For instance, a number 0.74 in the box says that 74% of the particles in that particular η and momentum range have been reconstructed fairly accurately. Therefore, it is evident from the figure that reconstruction is relatively poor in the negative rapidities beyond -3. It is compelling to note that the scattered electron falls mostly in those regions, as shown in Figure 5.10.

Similar study was done on the GEANT4 detector simulation to check the tracking efficiency as well, and the observations were no different. With these limitations, passing Sartre events through the GEANT4 full detector in order to carry out the reconstruction after matching the calorimeter and tracking data for each of the final state particles, was incapable of producing useful output; however, there are ongoing projects on improving the detector setup in GEANT4, by which the various detector subsystems can be modified to yield more

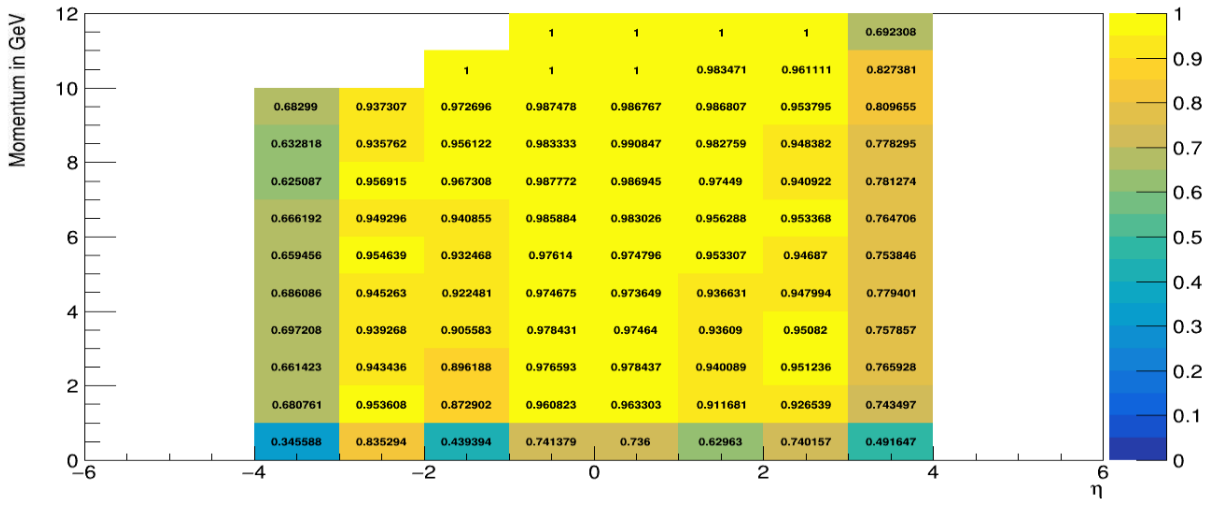

Figure 5.11: A 2D plot showing efficiency of the calorimeters in different pseudorapidities. The plot is made throwing 100,000 electrons uniformly between -4 $< \eta <$ +4 and momentum between 1 and 12 GeV.

accurate reconstruction, and, integrating it with the far forward detectors.

5.4 Phase space Analysis

At EIC, the possible energy configurations are [19];

- e + p beam energy configurations: 18x275, 10x275, 10x100, 5x100
- e + A beam energy configurations: 18x100, 10x100, 5x100
- 10 fb^{-1} integrated luminosity
- 70% polarization for both electrons and protons

With these configurations we will be able to access a wide variety of physics regimes and assess various physics studies.
In this section, we will see some analysis plots for ep and eA collisions in different kinematic phase space. The following figure (Figure 5.12) shows isolines of the scattered electron's angle and energy, and those of the hadronic final state for a centre of mass energy of $\simeq$

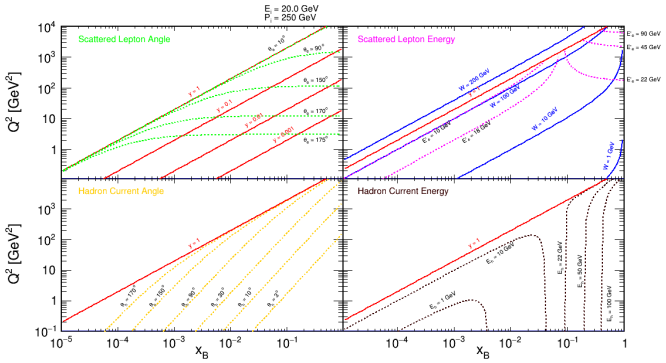

(a) ep collisions phase space analysis in $x - Q^2$ plane

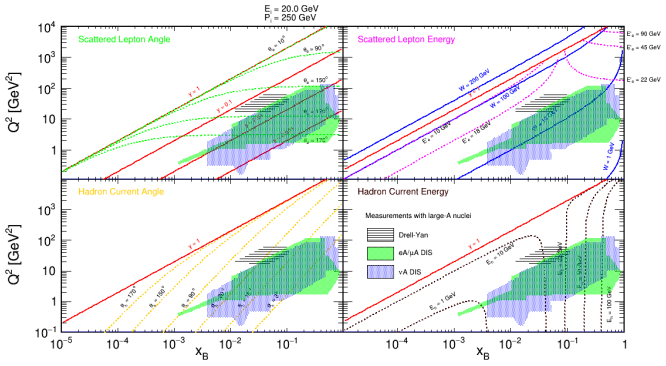

(b) eA collisions phase space analysis in $x - Q^2$ plane

Figure 5.12: Isolines of different variables used in various reconstruction methods shown in $x - Q^2$ plane [33]

140 GeV in ep (Figure 5.12 (a)) and eA (Figure 5.12 (b)) collisions in $x - Q^2$ plane. The importance of these isolines is that we can deduce a rough idea about the sensitivity of the various reconstruction methods which are based on these variables.
Let's carefully look at the isolines for scattered electron's energy and angle as shown in the first rows of the two figures in Figure 5.12. In the regions of $x - Q^2$ plane where these lines are closer, the errors in reconstructing these values do not have a significant effect on the reconstruction of kinematic variables using the Scattered Electron method or Double Angle method. However, in areas where the lines are separated, small errors might lead to big errors in kinematic reconstruction. The red lines correspond to constant y. We also realize that at lower y values, kinematics is mostly controlled by scattered electron's angle[34]. We see that the scattered electron carries very high energy at high Q^2. Similarly, in the rows below, the sensitivity of DA and JB methods to hadronic final state's energy and effective angle can be gathered. At intermediate x values, the hadronic energy varies highly with Bjorken x. At higher x, there is a highly energetic hadronic final state and much of the energy is emitted in the forward direction. In Figure 5.12 (b), we can also see real data from several experiments distributed in the same plane. From these plots, we see the different kinematic coverage of various deep inelastic scattering processes. These plots are also helpful in identifying kinematic cuts for various physics analysis.

5.5 Comparison of reconstruction methods

Given the resolutions of each of these variables in different kinematic regimes and accessibility to the calorimeter, tracking and particle identification of various final state particles, we have a flexible choice for event kinematic reconstruction methods.
As discussed previously, the Scattered Electron method gives fairly accurate reconstruction as compared to JB and DA methods. Hence, this result imposes detector requirements on EEMC and tracking in the electron going direction. In those CC events where we do not have a final state electron, but a neutrino which escapes detection, the only possible method of reconstruction is JB. The greatest advantage of using DA method for reconstruction is its independence on the final state energies as it depends on the ratio and hence, less sensitive to the systematic errors in reconstruction of calorimeter energies.
Since reconstruction using the Scattered Electron method depends on the incident energy of electron, it is sensitive to initial state radiation, ie, the photon bremsstrahlung of the

incoming electron. From the following equations [26][28],

$$\begin{aligned}
\frac{\delta Q_e^2}{Q_e^2} &= \frac{\delta E'_e}{E'_e} + tan\left(\frac{\theta_e}{2}\right).\delta\theta_e \\
\frac{\delta x_e}{x_e} &= \frac{1}{y}.\frac{\delta E'_e}{E'_e} + \left[\frac{(1-y_e)}{y_e}.cot\left(\frac{\theta_e}{2}\right) + tan\left(\frac{\theta_e}{2}\right)\right].\delta\theta_e \\
\frac{\delta y_e}{y_e} &= \left(1-\frac{1}{y_e}\right).\frac{\delta E'_e}{E'_e} + \left(\frac{1}{y_e}-1\right).cot\left(\frac{\theta_e}{2}\right).\delta\theta_e
\end{aligned} \tag{5.6}$$

we see that the resolutions in Q^2 and x calculated using electron method is highly dependent on the scattering angle. At smaller y, the uncertainty in x_e diverges. Similarly, the uncertainty in y_e becomes worse at smaller y due to the $\frac{1}{y_e}$ term in Equation 5.6. Hence, the methods which rely on hadronic final states are used for lower y. Also, the term $tan\left(\frac{\theta_e}{2}\right).\delta\theta_e$ becomes very large at large scattering angles, ie, when the electrons are back scattered, hence demanding detector requirements in the backward regions. Q_e^2 does not have any term which blows up, therefore gives accurate reconstruction over the full kinematic range.
Similarly for the hadronic final states,

$$\begin{aligned}
\frac{\delta Q_h^2}{Q_h^2} &= \frac{(2-y_h)}{(1-y_h)}.\frac{\delta E_h}{E_h} + \left[2cot\gamma_h + \frac{y_h}{1-y_h}.cot\left(\frac{\gamma_h}{2}\right)\right].\delta\gamma_h \\
\frac{\delta x_h}{x_h} &= \frac{1}{(1-y_h)}.\frac{\delta E_h}{E_h} + \left[-2cot\gamma_h + \frac{(1-2y_h)}{(1-y_h)}.cot\left(\frac{\gamma_h}{2}\right)\right].\delta\gamma_h
\end{aligned} \tag{5.7}$$

Unlike the reconstruction based on scattered electron, the Q^2 and x calculated using this method are largely dependent on y and the uncertainties in both of the quantities becomes sizable as y approaches 1. Hence, both ways of reconstruction, based on electron and hadron final states, are complementary to each other; DA method is a mixture of the two.
To summarize;

- The Scattered Electron Method gives fairly accurate reconstruction as compared to DA and JB methods; as we see in the studies at generator level as well as with detector smearing. (Figure 5.7)

- For the hadronic methods, some of the detected particles may originate from the remnant nucleus. However, if their momenta are primarily along the beam line, they will have a minimal effect on the kinematic variables (which depend on Σ_h).

- Electron method is ideal at larger y while hadronic method at lower y.
- At higher Q^2, JB and DA reconstruction seem to improve significantly.
- Including the outgoing proton as a part of the hadronic final state, improves the accuracy of reconstruction using JB and DA methods to a fair amount.(Figure 5.7 and Figure 5.8)
- In hadronic methods, while JB method gives a better reconstruction in y, DA method provides better Q^2 reconstruction in all kinematic regimes. (Figure 5.8)
- At smaller Q^2 regimes, DA method gives equally good or sometimes better resolution than Scattered Electron method for x and Q^2 reconstruction.(Figure 5.7)

Chapter 6

Summary and Outlook

This thesis work was focused on the reconstruction of event kinematics of the exclusive diffractive processes at EIC. These processes are observed as an important tool for understanding the gluon saturation, spatial distribution of gluons and, exploring a variety of other physics goals at EIC. Understanding the kinematics of events would give hints to measuring the structure function of hadrons in a deep inelastic scattering. Also, reconstruction of the kinematic variables is crucial in understanding the underlying physics process.

Sartre - the event generator for exclusive diffractive processes gives the true kinematics of the final state particles. The generator did not take into account the polarization effect of the virtual photon on the decay angular distribution of the vector meson in the DVMP process. However, several studies (including those on the HERA experiment) in the past, suggest a dependence of polarization of the virtual photon on the decay angular distribution of the vector meson based on the s-channel helicity conservation (SCHC). Initial studies for the thesis using Sartre kinematics and understanding the polarization effects on the decay angle, sparked curiosity to implement these effects in the generator. Hence, the Sartre generator is modified including the polarization effects of the vector meson.

The event kinematic reconstruction at generator level showed that the Scattered Electron Method is highly correlated with the true kinematic quantities. As the scattered electron has to be identified and reconstructed properly so as to get an accurate reconstruction using the Scattered Electron Method, later studies took the path to see if the J/ψ daughter

electron had any chance of being misidentified as the scattered electron. Referring to the EIC-sPHENIX prospective design as per the LOI 2018, different scenarios were considered and looked at the cases where the η of the electrons overlapped. Further analysis showed a very significant separation of these two electrons in the ϕ space. To get a more realistic picture, these electrons were projected onto the detector to calculate the physical separation between them which turned out to be of the order of centimetres while the electromagnetic calorimeters have far better resolution with higher granularity. The study showed that in an exclusive diffractive process, the J/ψ decay products are far separated from the scattered electron, thus improving the chances of accurate identification of the primary electron for the reconstruction studies and, giving a physical threshold for the granularity of the electromagnetic calorimeters.

Another careful observation of the reconstruction studies done at generator level led to the understanding of how crucial it is to detect the scattered proton in an exclusive *ep* diffractive process. The reconstruction using Jacquet Blondel and Double Angle methods improved significantly in resolution, when the properties of the outgoing proton were also considered in the final hadronic state summation. Therefore, in the eic-smear studies, Roman pots (for detecting protons) and ZDC (for detecting neutrons) were added to the existing setup, in addition to the central detector with the tracking system, and smeared the outgoing proton's transverse momentum. By doing so, the eic-smear is able to differentiate coherent and incoherent diffractive processes based on the hits on the ZDC, as neutrons are produced only in incoherent processes. Simulations show that placing roman pots at varying distances from the nominal collision point does not seem to affect their acceptance to the outgoing proton. On the other hand, studies made varying the angular acceptances of the roman pots show that most of the protons get scattered at angles $\leq$ 5mrad (in the diffractive processes generated at low Q^2) and, the roman pots with acceptance $2 \leq \eta \leq 15$mrad would provide a prospective measure for the size of the roman pots at EIC. Reconstruction of the event kinematic variables were done, using all the three methods, and agreed with the results from the generator level. To get a more realistic picture, full GEANT4 detector simulation studies were also done which led to a detailed understanding of the efficiencies and performance of the various detector subsystems in GEANT4 detector simulation. As the GEANT4 has only the central detector system implemented, reconstruction comparisons with and without including the outgoing proton in JB and DA methods could not be covered.

Thus, the thesis work provides a detailed study on event kinematic reconstruction of exclusive diffractive vector meson production in both ep and eA collisions. The results agree with the past studies that the Scattered Electron Method gives the most accurate reconstruction of the kinematic variables as compared to the Jacquet Blondel and Double Angle methods. At high x, y or Q^2, both the Scattered Electron method and Double Angle method have comparable resolutions. While the electron method works better at low x, Q^2, the double angle method works better at lower y. The Jacquet Blondel method gives relatively poor resolution in x and Q^2 as compared to the other two methods, in low x - Q^2 regimes. The higher the Q^2 of the process, the reconstruction using the Jacquet Blondel and the Double Angle gets better. These studies are crucial for various aspects in the detector design.

6.1 Outlook

- As the eic-smear package uses various approximations for fast smearing of various detector subsystems, a careful study on the resolutions required by each detector will lead to modifying the existing resolution and provide a better picture in a very fast simulation.
- There are ongoing projects focusing on improving the accuracy of the GEANT4 detector simulation of the central EIC-sPHENIX detector. Also, GEANT4 simulation studies can be improved if the far-forward detectors can also be added to the simulation. EicRoot is a specific package for the far-forward detectors based on GEANT3 and can be integrated with the GEANT4 setup of central detector. A lot of interesting physics studies using the scattered DVCS proton and/or nucleus can be conducted based on the simulations using this integrated detector system.

Bibliography

[1] M. Planck, Verh. Deutsch. Phys. Ges. **2**, 237 (1900).

[2] A. Einstein, AdP **49**, 54 (1916)

[3] E. Rutherford, Phil. Mag. **21**, 669 (1911)

[4] J. Chadwick, Proc. Roy. Soc. A 136, 692 (1932).

[5] TASSO Coll., R. Brandelik et al., Phys. Lett. **B86**, 243 (1979);
D. P. Barber et al., Phys. Rev. Lett. **43**, 830 (1979);
PLUTO Coll., C. Berger et al., Phys. Lett. **B86**, 418 (1979);
JADE Coll., W. Bartel et al., Phys. Lett. **B91**, 142 (1980).

[6] R.P. Feynman, *Photon-Hadron Interactions*. Benjamin, New York, 1972

[7] E. D. Bloom et al., Phys. Rev. Lett. 23, 930 (1969); M. Breidenbach et al., Phys. Rev. Lett. 23, 935 (1969).

[8] Alan Martin and Francis Halzen. *Quarks and Leptons: An Introductory Course in Modern Particle Physics*. John Wiley and Sons, 1984.

[9] Thomson, Mark. *Modern Particle Physics.*

[10] A. Accardi et al. Electron Ion Collider: The Next QCD Frontier. Eur. Phys. J., A52 (9):268, 2016. doi: 10.1140/epja/i2016-16268-9.

[11] Reaching for the Horizon: The 2015 Long Range Plan for Nuclear Science. 2015.
URL `https://science.energy.gov/~/media/np/nsac/pdf/2015LRP/2015_LRPNS_091815.pdf`

[12] Abhay Deshpande, Science and status of the Electron Ion Collider.
doi: 10.1142/S0218301317400079

[13] EIC Monte Carlo and Smearing Wiki page.
URL `https://wiki.bnl.gov/eic/index.php/Monte_Carlo_and_Smearing.`

[14] Eicroot Wiki page
URL https://wiki.bnl.gov/eic/index.php/Eicroot

[15] An EIC Detector Built Around The sPHENIX Solenoid. A Detector Design Study. 2018.

[16] Site for EIC. URL https://www.bnl.gov/newsroom/news.php?a=116998

[17] Heikki Mantysaari. Photoproduction prospects at the EIC. arXiv:1708.05756 [nucl-ex].

[18] Ursula Bassler, Gregorio Bernardi. On the Kinematic Reconstruction of Deep Inelastic Scattering at HERA: the Σ Method. arXiv:9412004 [hep-ex]

[19] EIC-SPHENIX Detector Design Study 2018.
URL https://wiki.bnl.gov/sPHENIX/index.php/EIC-SPHENIX_Detector_Design_Study_2018

[20] Tobias Toll, Thomas Ullrich. The dipole model MonteCarlo generator Sartre1 arXiv:1307.8059 [hep-ph]

[21] Michael Lomnitz, Spencer Klein. Exclusive vector meson production at an electron-ion collider. arXiv:1803.06420 [nucl-ex]

[22] C. Adloff, et al. (H1 Collaboration) Elastic Electroproduction of rho Mesons at HERA. arXiv:9902019 [hep-ex]

[23] M. Klein, R. Yoshida. Collider Physics at HERA. arXiv:0805.3334 [hep-ex]

[24] eRHIC Design Study- An Electron-Ion Collider at BNL. arXiv:1409.1633

[25] Yulia Furletova. EIC Status- Detector and Simulations.
URL https://www.jlab.org/hugs/HUGS-DET1.pdf

[26] M. Klein, R. Yoshida, Collider Physics at HERA. arXiv:0805.3334 [hep-ex]

[27] E C Aschenauer, S Fazio, J H Lee, H Mäntysaari, B S Page, B Schenke, T Ullrich, R Venugopalan, P Zurita,The Electron-Ion Collider: Assessing the Energy Dependence of Key Measurements. arXiv:1708.01527 [nucl-ex]

[28] Vladimir Vladimirovich Arkadov, Measurement of the Deep Inelastic ep Scattering Cross Section using the Backward Silicon Tracker at the H Detector at HERA1111 URL https://www-h1.desy.de/psfiles/theses/h1th-226.pdf

[29] Charles E Hyde.
https://indico.bnl.gov/event/6799/contributions/34181/attachments/26351/39827/CHyde_FarForward.pdf

[30] Grijpink, S.J.L.A. Charged Current Cross Section Measurement at HERA.
URL https://pure.uva.nl/ws/files/3595849/39237_Thesis.pdf

[31] Ursula Bassler, Gregorio Bernardi, On the Kinematic Reconstruction of Deep Inelastic Scattering at HERA: the Σ Method arXiv:9412004 [hep-ex]

[32] N.C.R. Makins, NNPSS 2011. Deep Inelastic Scattering.
URL http://www.tunl.duke.edu/nnpss/lectures/11/NNPSS11-2-nobuilds.pdf

[33] Dr. Barak Schmookler, private communication.

[34] Rainer Thomas Ullmann, Neutral Strange Particle Production in Neutral Current Deep Inelastic Scattering at HERA
URL https://www.collectionscanada.gc.ca/obj/s4/f2/dsk2/ftp02/NQ30407.pdf

[35] C. Diaconu. The physics of Deep Inelastic Scattering at HERA.
URL http://www.nipne.ro/rjp/2007_52_9-10/0941_0991.pdf